Closed-Loop Cadence and Instantaneous Power Control on a Motorized Functional Electrical Stimulation Cycle

Christian A. Cousin[©], Victor H. Duenas[©], Courtney A. Rouse[©], Matthew J. Bellman, Paul Freeborn, Emily J. Fox, and Warren E. Dixon[©]

Abstract—Motorized functional electrical stimulation (FES) cycling is a rehabilitation therapy in which electrical stimulation is used to activate lower body muscles to pedal a cycle in conjunction with motorized assistance. FES cycling has been demonstrated to improve cardiovascular parameters, muscle mass, and motor control of people with neurological conditions (NCs). A common FES cycling objective is simultaneous cadence and power (torque) tracking; however, it is unclear how to best coordinate the FES and motor contributions and if power should be tracked instantaneously or averaged over a period of time. This article develops a new FES cycling controller using a switched Lyapunov-like dwell-time analysis for the nonlinear, uncertain cycling system to conclude global exponential cadence tracking and uniformly ultimately bounded power tracking. To evaluate the performance of the developed controller, comparisons are made with two previously developed FES cycling controllers through experiments on seven able-bodied participants and six participants with NCs. For a desired cadence of 50 RPM and a desired power of 10 W, the developed controller demonstrated the smallest tracking errors with an average cadence and power error of 0.01±1.03 RPM and 0.00±0.94 W, respectively, in the able-bodied population and an average cadence and power error of 0.02±1.87 RPM and 0.00±2.46 W, respectively, in the population of people with NCs. Results suggest that the electric motor should be used to track cadence and the FES induced muscle torques should be used to track instantaneous power.

Index Terms—Functional electrical stimulation (FES), Lyapunov, nonlinear control, power tracking, rehabilitation, switched system.

Manuscript received April 20, 2018; revised April 5, 2019 and July 24, 2019; accepted July 26, 2019. Date of publication September 19, 2019; date of current version October 9, 2020. Manuscript received in final form August 22, 2019. This work was supported in part by NSF under Award DGE-1842473, Award DGE-1315138, and Award 1762829. Recommended by Associate Editor A. Serrani. (Corresponding author: Christian A. Cousin.)

- C. A. Cousin is with the Department of Mechanical Engineering, The University of Alabama, Tuscaloosa, AL 35401 USA (e-mail: cacousin@eng.ua.edu).
- V. H. Duenas is with the Department of Mechanical and Aerospace Engineering, Syracuse University, Syracuse, NY 13244 USA (e-mail: vhduenas@syr.edu).
- C. A. Rouse, M. J. Bellman, and W. E. Dixon are with the Department of Mechanical and Aerospace Engineering, University of Florida, Gainesville, FL 32611 USA (e-mail: courtneyarouse@ufl.edu; mattjo@ufl.edu; wdixon@ufl.edu).
- P. Freeborn is with the Brooks Rehabilitation Motion Analysis Center, Jacksonville, FL 32216 USA (e-mail: paul.freeborn@brooksrehab.org).
- E. J. Fox is with the Brooks Rehabilitation Motion Analysis Center, Jacksonville, FL 32216 USA, and also with the Department of Physical Therapy, University of Florida, Gainesville, FL 32610 USA (e-mail: emily.fox@brooksrehab.org).

Color versions of one or more of the figures in this article are available online at http://ieeexplore.ieee.org.

Digital Object Identifier 10.1109/TCST.2019.2937725

I. INTRODUCTION

EHABILITATIVE therapies can lead to significant Mimprovements in the activities of daily living for people with movement impairments due to neurological conditions (NCs) such as stroke, spinal cord injury (SCI), traumatic brain injury (TBI), cerebral palsy (CP), multiple sclerosis (MS), and others. Such NCs can reduce a person's strength, endurance, or limb control, mitigating their ability to voluntarily achieve certain functional tasks or the associated desired training effects. A common rehabilitation option for movement impairments is to coordinate limb motions by eliciting muscle contractions through functional electrical stimulation (FES). For example, FES of the lower body muscles is often used by therapists to facilitate cycling tasks (along with motorized assistance), yielding improvements in musculoskeletal and cardiorespiratory fitness as well as other neurological, physiological, and psychological measures [1]-[3].

Stationary FES cycling is a popular rehabilitative therapy because fall risks associated with other therapies are mitigated, it can provide sufficient intensity and repetitive practice of coordinated limb movements critical for facilitating nervous system reorganization, and promote potential beneficial changes in the neuromuscular system [4], [5]. However, the metabolic efficiency of FES cycling is significantly lower than volitional cycling [6] due to poor control of the muscle groups, unfavorable biomechanics and nonphysiological muscle recruitment [7], non-optimal stimulation parameters [8], [9], fatigue [10]-[12], and other factors (see [13]-[15]). Increasing the efficiency and power output (PO) of FES cycling is desirable because it can reverse muscle atrophy and cultivate fatigue resistant muscle fibers [10], increase cardiovascular parameters [15], and provide additional health benefits (see [7], [8], [12], [16]). Multiple strategies have been employed to increase the PO of FES cycling such as cadence strategies [7], [14], creating the optimal pedal path [8], releasing the ankle joint [13], using a fixed gear cycle [17], using higher stimulation currents [10], and modifying the stimulation frequency and pattern [9]. Although FES cycling has been used as a rehabilitative therapy for decades, it has gained recent attention due to events such as the Cybathalon FES cycling race. Given the nature of the event, all racers used open-loop methods or rider controlled parameters [18], where the efficiency advantages of implanted electrodes were demonstrated by the winning team in 2016.

1063-6536 © 2019 IEEE. Personal use is permitted, but republication/redistribution requires IEEE permission. See https://www.ieee.org/publications/rights/index.html for more information.

From a control systems perspective, FES cycling is an example of a switched system in the sense that there are continuous physical dynamics of the limbs and the cycle, yet there are discrete logical jumps necessary to engage different muscle groups of the legs, potentially engage a motor for assistance, or discretely turn on/off the control (motivated by different stimulation schemes or the desire to allow the rider to contribute all the torque). However, few results consider the fact that such switching could yield degraded performance or even destabilizing effects. Although past FES cycling studies have been produced which control FES cycles using open-loop methods [19], or closed-loop methods such as linear [20] or nonlinear control techniques (e.g., fuzzy logic, sliding mode) [21], generally, the FES-cycling community has only addressed the ramifications of having a switched input by examining different regions to activate the muscle if at all (see [7], [19], [22]-[24]). The only control developments that are based on a nonlinear stability analysis that considers the impacts of switching during FES cycling are [25]-[28] and our precursory results in [29] and [30], which led to the current result, and investigates switched systems tools for simultaneous cadence and power tracking.1 Based on the idea that the limited bandwidth of electrically stimulated muscle groups inhibits torque tracking, few torque/power tracking results are available for instantaneous torque tracking (see [20], [21], [29]), discretized torque tracking (see [30], [31]) (which periodically updates the controller based on a power reading averaged over a region of the crank), or track power only when kinematically efficient (see [27]), and instead analyze PO outside the control loop (see [15], [19], [32]).

Compared to our recent work in [28], which utilizes a repetitive learning controller to track a time-periodic cadence trajectory, this article and the associated precursory results in [29] and [30], examine simultaneous cadence and power tracking for an uncertain nonlinear FES cycle using Lyapunov-based and switched systems analysis tools, including a dwell-time analysis. From a rehabilitation perspective, power tracking is desirable in the sense that high PO can help to prevent muscle atrophy, delay fatigue, increase cardiovascular parameters and provide additional health benefits [7], [8], [10], [12], [15], [16]. Building on the development in [29], a running integral is employed to allow for instantaneous power tracking. In addition, the effect of switching between different actuators is considered for both cadence and power tracking objectives using a novel Lyapunov-like switched system stability analysis, which yields global exponential cadence tracking and uniform ultimately bounded (UUB) power tracking. This article updates the power tracking error instantaneously, compared to once per crank cycle as in [30], and heuristically is better able to accommodate for rider asymmetries because each leg receives a unique stimulation pattern, compared to each leg receiving the same pattern, as in [30]. Furthermore, the electric motor is used for cadence tracking, which is the opposite strategy of the development in [29].

Experiments are conducted on seven able-bodied participants and six participants with NCs. The experimental results

¹Within the scope of this work, power tracking and torque tracking are synonymous. provide insights for open questions related to the coordination between the contributions made by FES and the electric motor and if power should be tracked instantaneously (as in this article) or averaged over a period of time (as is typical in practice). Specifically, the experimental results from the instantaneous power tracking controller in this article showed improvements over the controllers in [29] and [30]. The comparison to the controllers in [29] and [30] provides insight into strategies for the division of effort between the electric motor and neuromuscular contributions, and into strategies that use instantaneous versus averaged torque feedback, respectively.

II. DYNAMICS

A. Cycle-Rider Dynamics

The combined cycle-rider dynamics are [26]2

$$\sum_{m \in \mathcal{M}} b_m(q, \dot{q}) u_m(t) + b_e u_e(t) = M(q) \ddot{q} + V(q, \dot{q}) \dot{q} + G(q) + P(q, \dot{q}) + b_c \dot{q} + d(t)$$
(1)

where $q: \mathbb{R}_{\geq 0} \to \mathcal{Q}, \dot{q}: \mathbb{R}_{\geq 0} \to \mathbb{R}$, and $\ddot{q}: \mathbb{R}_{\geq 0} \to \mathbb{R}$ denote the crank angle (measurable), velocity (calculable), and acceleration, respectively. The set of $Q \subseteq \mathbb{R}$ denotes the possible angles of the crank. The torques applied about the crank axis by the combined inertial, centripetal-Coriolis, and gravitational effects are denoted by $M: \mathcal{Q} \to \mathbb{R}_{>0}$, $V: \mathcal{Q} \times \mathbb{R} \to \mathbb{R}$, and $G: \mathcal{Q} \to \mathbb{R}$, respectively, and the torques applied about the crank by the rider's passive viscoelastic tissue forces are denoted by $P: \mathcal{Q} \times \mathbb{R} \to \mathbb{R}$. The viscous damping effects applied by the cycle are denoted by $b_c: \mathbb{R}_{\geq 0} \to \mathbb{R}$ and unmodeled disturbances are denoted by $d: \mathbb{R}_{\geq 0} \to \mathbb{R}$. The inputs to the system include the rider's primary leg muscle groups (activated via FES) and the cycle's electric motor coupled to the drive chain. The torque applied by the rider's muscles is defined as $\tau_m: \mathcal{Q} \times \mathbb{R} \times \mathbb{R}_{\geq 0} \to \mathbb{R}$, and is the product of the uncertain muscle control effectiveness,3 denoted by $b_m: \mathcal{Q} \times \mathbb{R} \to \mathbb{R}_{>0}$, and the subsequently designed FES muscle control current input, $u_m : \mathbb{R}_{\geq 0} \to \mathbb{R}$, summed across the muscle groups [i.e., $\tau_m \triangleq \sum_{m \in \mathcal{M}} b_m(q, \dot{q}) u_m(t)$]. The subscript $m \in \mathcal{M} \triangleq \{RQ, RG, RH, LQ, LG, LH\}$ indicates the right (R) and left (L) quadriceps femoris (Q), gluteal (G), and hamstring (H) muscle group, respectively, which denote the stimulated muscle groups.

The torque applied by the cycle's electric motor is defined as $\tau_e : \mathbb{R}_{\geq 0} \to \mathbb{R}$, and is the product of the known motor control constant, $b_e \in \mathbb{R}_{>0}$, and the subsequently designed motor control current input, $u_e : \mathbb{R}_{\geq 0} \to \mathbb{R}$ [i.e., $\tau_e \triangleq b_e u_e(t)$].⁴

B. Switched System

As in results such as [25], [26], [30], FES-cycling is accomplished by switching the stimulation input to different muscle groups based on the region of the crank cycle (i.e., the FES

²For notational brevity, all explicit dependence on time, t, within the terms q(t), $\dot{q}(t)$, $\ddot{q}(t)$ is suppressed.

³Although the muscle control effectiveness includes dynamic effects such as fatigue and electromechanical delay, they are not captured within the dynamics presented but instead addressed in Section V-B.

⁴For notational brevity, all functional dependence on system states and time are hereafter suppressed unless required for clarity of exposition.

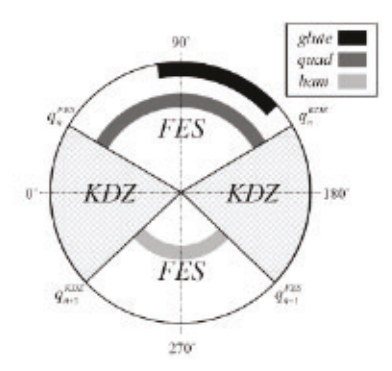


Fig. 1. Sample crank cycle illustrating the FES and KDZ regions. Highlighted within the FES regions are the regions where it is efficient to stimulate the gluteals (glute), quadriceps (quad), and hamstrings (ham). Crank positions $q_n^{\rm FES}$ and $q_n^{\rm KDZ}$ denote the points at which the crank enters the FES and KDZ regions of cycle n, respectively. Cycle n refers to the nth time the crank enters the FES region. Image reproduced from [25].

regions) designed a priori based on the kinematic effectiveness of the torque transferred to the crank axis from the muscle. In regions of the crank where it is inefficient to stimulate muscle, a kinematic deadzone (KDZ) region exists and no muscle stimulation is applied. The stimulation regions are based on the work in [26], denoted by $Q_m \subset Q$, and designed such that backpedaling is prevented and stimulation is only applied when each muscle group can positively contribute to the motion of the crank. The union of all muscle regions establishes the FES region, defined as $Q_{\text{FES}} \triangleq \bigcup_{m \in \mathcal{M}} Q_m$, and the KDZ region as the remainder of the crank cycle, i.e., $Q_{\text{KDZ}} \triangleq Q \setminus Q_{\text{FES}}$. The FES and KDZ regions are depicted in Fig. 1.

The stimulation input to the muscle groups and the current input to the electric motor are defined as

$$u_m \triangleq k_m \sigma_m u_{tor}$$
 (2)

$$u_e \triangleq k_e u_{cad}$$
 (3)

where k_m , $k_e \in \mathbb{R}_{>0}$ are positive constant control gains, u_{tor} , $u_{\text{cad}} : \mathbb{R}_{\geq 0} \to \mathbb{R}$ denote the subsequently designed control inputs for the muscle and motor, respectively, and $\sigma_m : Q \to \{0, 1\}$ denotes the switching signal for each muscle group, defined as

$$\sigma_m \triangleq \begin{cases} 1, & q \in Q_m \\ 0, & q \notin Q_m \end{cases}$$
(4)

 $\forall m \in \mathcal{M}$. Substituting (2) and (3) into (1) and rearranging terms yields the switched system

$$B_{\sigma}u_{\text{tor}} + B_{\varepsilon}u_{\text{cad}} = M\ddot{q} + V\dot{q} + G + P + b_{c}\dot{q} + d \qquad (5)$$

where $B_{\sigma}: \mathcal{Q} \times \mathbb{R} \to \mathbb{R}$ is the combined, switched control effectiveness muscle term, and $B_{e} \in \mathbb{R}_{>0}$, is the control effectiveness motor term, each defined as

$$B_{\sigma}(q,\dot{q}) \triangleq \sum_{m \in \mathcal{M}} b_m k_m \sigma_m$$
 (6)

$$B_a \triangleq b_a k_a$$
 (7)

respectively. The index of B_{σ} , $\sigma: \mathcal{Q} \to \{1, 2, ..., l\}$, $l \in \mathbb{N}$ specifies which muscle groups(s) are stimulated, where l denotes all the possible permutations of stimulated muscle groups. The switched system in (5) has the following properties [26].

Property 1: $c_m \leq M \leq c_M$, where c_m , $c_M \in \mathbb{R}_{>0}$ are known constants. Property 2: $|V| \le c_V |\dot{q}|$, where $c_V \in \mathbb{R}_{>0}$ is a known constant. Property 3: $|G| \le c_G$, where $c_G \in \mathbb{R}_{>0}$ is a known constant. Property 4: $|P| \le c_{P1} + c_{P2}|\dot{q}|$, where $c_{P1}, c_{P2} \in \mathbb{R}_{>0}$ are known constants. Property 5: $b_c \leq c_b$, where $c_b \in \mathbb{R}_{>0}$ is a known constant. Property 6: $|d| \le c_d$, where $c_d \in \mathbb{R}_{>0}$ is a known constant. Property 7: M-2V = 0, by skew-symmetry. Property 8: The uncertain muscle control effectiveness, b_m , is subject to nonlinear activation dynamics and a muscle fiber recruitment curve (commonly represented by sigmoidal function) [33], [34]. Based on [35], the function relating the stimulation input current to output torque is bounded by $b_{\underline{m}} \leq b_{\overline{m}}, \forall m \in \mathcal{M}$, where $b_m, b_m \in \mathbb{R}_{>0}$ are known constants. Hence, when $q \in$ Q_{FES} (i.e., $\sum_{m \in \mathcal{M}} \sigma_m > 0$), the lumped switched control effectiveness term is also bounded by $B_{\sigma} \leq B_{\sigma} \leq B_{\overline{\sigma}}$, where B_{σ} , $B_{\overline{\sigma}} \in \mathbb{R}_{>0}$ are known constants.

C. Torque Dynamics

The dynamics in (1) can be rewritten as

$$\tau_m + \tau_e = \tau_p + \tau_c \tag{8}$$

where the torques applied about the crank axis by the rider's muscles, the electric motor, the rider's passive effects, and the cycle are denoted by $\tau_m: \mathcal{Q} \times \mathbb{R} \times \mathbb{R}_{\geq 0} \to \mathbb{R}$, $\tau_e: \mathcal{Q} \times \mathbb{R} \times \mathbb{R}_{\geq 0} \to \mathbb{R}$, $\tau_p: \mathcal{Q} \times \mathbb{R}^2 \to \mathbb{R}$, and $\tau_c: \mathbb{R}^2 \times \mathbb{R}_{\geq 0} \to \mathbb{R}$, respectively. Motivated by the need to separate the torque contribution of the motor and muscles, when no stimulation is applied, $\tau_m \equiv 0$, and (8) simplifies to

$$\tau_{\text{est}} = \tau_p + \tau_c$$
 (9)

where $\tau_{\text{est}}: \mathcal{Q} \times \mathbb{R}^2 \times \mathbb{R}_{\geq 0} \to \mathbb{R}$ is an auxiliary term defined as $\tau_{\text{est}} \triangleq \tau_{e}$ when no stimulation is applied. The structure of (9) is motivated by the fact that τ_{p} and τ_{c} represent the passive rider and cycle dynamics, respectively, which are amenable to pretrial estimation. Based on the structure of (9), the following assumptions are made.

Assumption 1: The disturbances and auxiliary terms are sufficiently smooth in the sense that \dot{d} , $\tau_{\rm est}$, $\dot{\tau}_{\rm est} \in \mathcal{L}_{\infty}$ [30].

Assumption 2: A continuously differentiable estimate of τ_{est} , denoted by $\hat{\tau}_{est}: \mathcal{Q} \times \mathbb{R}^2 \times \mathbb{R}_{\geq 0} \to \mathbb{R}$, can be generated during preliminary testing such that the estimate error, $\tilde{\tau}_{est}: \mathcal{Q} \times \mathbb{R}^2 \times \mathbb{R}_{\geq 0} \to \mathbb{R}$ defined as

$$\tilde{\tau}_{\text{est}} \triangleq \hat{\tau}_{\text{est}} - \tau_{\text{est}}$$
 (10)

is bounded by $|\tilde{\tau}_{\rm est}| \leq c_{\rm est}$, where $c_{\rm est} \in \mathbb{R}_{\geq 0}$ is a known constant. This assumption is reasonable provided no stimulation is applied during preliminary testing (i.e., $\tau_m = 0$), the disturbances are sufficiently small when $\tau_{\rm est}$ is generated, and the desired trajectory is the same during the generation of $\tau_{\rm est}$ and the actual experimental trial [30].

The muscle torque can be rewritten by subtracting $\hat{\tau}_{est}$ from (8) and using (10) as

$$\tau_m = \hat{\tau}_{cst} - \tau_{\epsilon} + \tilde{\tau}_{cst}. \tag{11}$$

Defining the estimate of the muscle torque, $\hat{\tau}_m: \mathcal{Q} \times \mathbb{R}^2 \times \mathbb{R}_{\geq 0} \to \mathbb{R}$, as

$$\hat{\tau}_m \triangleq \hat{\tau}_{est} - \tau_e$$
 (12)

and subtracting (12) from (11) yields the muscle torque estimation error, $\tilde{\tau}_m: \mathcal{Q} \times \mathbb{R}^2 \times \mathbb{R}_{>0} \to \mathbb{R}$, defined as

$$\tilde{\tau}_m \triangleq \hat{\tau}_m - \tau_m$$
 (13)

which can be bounded by $|\tilde{\tau}_m| \le c_{\text{est}}$, where c_{est} was defined in Assumption 2.

III. ERROR SYSTEM DEVELOPMENT

A. Position and Cadence Error Systems

The position tracking objective is quantified by $e_1 : \mathbb{R}_{>0} \to \mathbb{R}$, defined as

$$e_1 \triangleq q_d - q$$
 (14)

where $q_d: \mathbb{R}_{\geq 0} \to \mathbb{R}$ denotes the desired angular trajectory which is sufficiently smooth (i.e., \dot{q}_d , $\ddot{q}_d \in \mathcal{L}_{\infty}$) and bounded by $q_d \leq c_{q0}$, $\dot{q}_d \leq c_{q1}$, and $\ddot{q}_d \leq c_{q2}$. To facilitate the control development and stability analysis, an auxiliary tracking error $e_2: \mathbb{R}_{\geq 0} \to \mathbb{R}$ is defined as

$$e_2 \triangleq \dot{e}_1 + \alpha e_1 \tag{15}$$

where $\alpha \in \mathbb{R}_{>0}$ is a constant control gain. Taking the derivative of (15), multiplying it by M, adding and subtracting e_1 , then substituting (5), (14), and (15) yields the open-loop cadence error system

$$M\dot{e}_2 = \chi_1 - e_1 - Ve_2 - B_e u_{cad} - B_\sigma u_{tor}$$
. (16)

The lumped auxiliary term, $\chi_1: \mathcal{Q} \times \mathbb{R} \times \mathbb{R}_{\geq 0} \to \mathbb{R}$, defined as $\chi_1 \triangleq M(\ddot{q}_d + \alpha \dot{e}_1) + V(\dot{q}_d + \alpha e_1) + G + P + b_c(\dot{q}_d + \alpha e_1 - e_2) + d + e_1$ can be upper bounded as $|\chi_1| \leq c_1 + c_2 ||z|| + c_3 ||z||^2$ by Properties 1-6, where c_1 , c_2 , $c_3 \in \mathbb{R}_{>0}$ are known the constants, defined as

$$c_1 \triangleq c_M c_{q2} + c_V c_{q1}^2 + c_G + c_{P1} + c_{P2} c_{q1} + c_b c_{q1} + c_d$$
(17)

$$c_2 \triangleq (c_M \alpha + c_{P2} + c_b)(\alpha + 1) + c_V c_{q1}(2\alpha + 1) + 1$$
 (18)

$$c_3 \triangleq c_V \alpha(\alpha + 1)$$
 (19)

where $\|\cdot\|$ denotes the standard Euclidean norm, and the error vector $z \in \mathbb{R}^2$ is defined as $z \triangleq [e_1, e_2]^T$.

B. Torque Error System

Compared to discrete torque (i.e., power) tracking, instantaneous torque tracking offers numerous benefits. With discretized tracking where the error system is updated once per crank cycle, the control input is updated once per crank cycle and result in both legs receiving identical stimulation. Such an approach fails to isolate the capabilities of either leg as the control input is based on the error generated from the contribution of both the legs as a whole. In addition, because the error is updated at the same point every cycle, the initially (i.e., soon after the error update) stimulated muscle groups receive a control input that reflects the error with little delay, but other muscle groups receive a considerably delayed input. Over the course of an experiment, this effect can culminate in one-sided fatigue and could potentially mitigate rehabilitation outcomes. For this reason, the torque tracking objective in this article is to prove that the estimated muscle torque instantaneously tracks the desired muscle torque (i.e., $\hat{\tau}_m \rightarrow \tau_{m,d}$), where $\tau_{m,d}: \mathbb{R}_{\geq 0} \to \mathbb{R}$ denotes the sufficiently smooth (i.e., $\tau_{m,d}$, $\dot{\tau}_{m,d} \in \mathcal{L}_{\infty}$) desired torque trajectory which is bounded by $\tau_{m,d} \leq c_{\tau 0}$ and $\dot{\tau}_{m,d} \leq c_{\tau 1}$. To facilitate the subsequent analysis, the torque tracking objective is represented as a integral, denoted by $e_3: \mathbb{R}_{\geq 0} \to \mathbb{R}$, and defined as [36]

$$e_3 \triangleq \int_{t_0}^t (\tau_{m,d}(\psi) - \hat{\tau}_m(\psi))d\psi$$
 (20)

where $t_0 \in \mathbb{R}_{\geq 0}$ represents the initial time, and the derivative of (20), given by

$$\hat{e}_3 = \tau_{m,d}(t) - \hat{\tau}_m(t) \tag{21}$$

represents the true torque tracking error. Motivated by the result in [36] and the subsequent stability analysis, the form of the tracking error in (20) was designed such that the subsequently designed torque controller is able to directly influence the derivative in (21), and hence, the closed-loop error system. Substituting (12) into (20) and taking its derivative, then inserting (2), (6), (8), and (9) yields the open-loop torque error system

$$\dot{e}_3 = \gamma_2 - B_\sigma u_{\text{tor}}. \tag{22}$$

The lumped auxiliary term, $\chi_2: Q \times \mathbb{R}^2 \times \mathbb{R}_{\geq 0}$, defined as $\chi_2 \triangleq \tilde{\tau}_{\text{est}} + \tau_{m,d}$, can be upper bounded as $|\chi_2| \leq c_4$ by Assumption 2, where $c_4 \in \mathbb{R}_{\geq 0}$ is a known constant defined as

$$c_4 \triangleq c_{\text{est}} + c_{\tau 0}. \tag{23}$$

C. Closed-Loop Error Systems

Based on (16), (22), and the subsequent stability analysis, the controllers are designed as

$$u_{\text{cad}} = \frac{1}{B_e} [(k_2 + k_3 ||z|| + k_4 ||z||^2 + k_5 |u_{\text{tor}}|) \operatorname{sgn}(e_2) + k_1 e_2]$$
(24)

$$u_{\text{tor}} = \frac{1}{B_{\sigma}} [k_6 e_3 + k_7 \text{sgn}(e_3)]$$
 (25)

where $k_i \in \mathbb{R}_{\geq 0} \ \forall i = 1, 2..., 7$ denote constant control gains and $sgn(\cdot) : \mathbb{R} \to [-1, 1]$ denotes the signum function. Substituting (24) and (25) into (16) and (22), respectively, yields the closed-loop error systems

$$M\dot{e}_{2} = \chi_{1} - e_{1} - Ve_{2} - B_{\sigma}u_{\text{tor}} - [(k_{2} + k_{3}||z|| + k_{4}||z||^{2} + k_{5}|u_{\text{tor}}|)\text{sgn}(e_{2}) + k_{1}e_{2}]$$
(26)

$$\dot{e}_3 = \chi_2 - \frac{B_\sigma}{B_\sigma} [k_6 e_3 + k_7 \text{sgn}(e_3)].$$
 (27)

The block diagram for the combined cycle-rider system is shown in Fig. 2.

IV. STABILITY ANALYSIS

To ensure overall system stability, both the cadence and torque error systems must be analyzed in the FES and KDZ regions along with analyzing the effect of switching between the subsystems. Because cadence is regulated with the electric motor throughout the entire crank cycle, switching

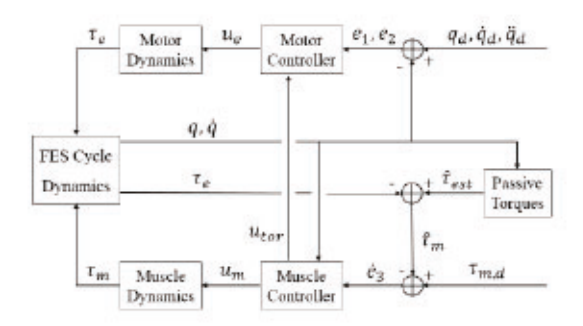


Fig. 2. Block diagram representing the closed-loop feedback structure of combined cycle-rider system. The muscle controller and the motor controller are given in (2) and (3), respectively. The muscle, motor, and FES cycle dynamics are modeled as in (1) and the passive torques are obtained according to Assumption 2.

occurs between stabilizable subsystems. Therefore, Theorem 1 includes a common Lyapunov function to demonstrate exponential cadence tracking for all time. Torque, however, is only regulated in the FES region using the rider's muscles; this leads to incomplete control authority and opportunities for error growth in the KDZ region. Theorems 2–4 include an additional candidate Lyapunov function that not only establishes an ultimate bound on the torque error system but also its derivative (i.e., the true torque objective). For the following analysis, let $V_1: \mathbb{R}^2 \to \mathbb{R}$ and $V_2: \mathbb{R} \to \mathbb{R}$ denote continuously differentiable, positive definite candidate Lyapunov functions defined as

$$V_1 \triangleq \frac{1}{2}e_1^2 + \frac{1}{2}Me_2^2 \tag{28}$$

$$V_2 \triangleq \frac{1}{2}e_3^2. \tag{29}$$

The candidate Lyapunov function V_1 satisfies the following inequalities:

$$|\underline{\lambda}||z||^2 \le V_1 \le \overline{\lambda}||z||^2 \tag{30}$$

where $\underline{\lambda}$, $\overline{\lambda} \in \mathbb{R}_{>0}$ are known constants defined as $\underline{\lambda} \triangleq \min((1/2), (c_m/2))$, $\overline{\lambda} \triangleq \max((1/2), (c_M/2))$.

Theorem 1: For $q \in \mathcal{Q}$, the closed-loop error system in (26) yields global exponential position and cadence tracking in the sense that

$$||z(t)|| \le \sqrt{\frac{\lambda}{\lambda}} ||z(t_n)|| \exp\left[-\frac{1}{2}\Lambda(t-t_n)\right]$$
 (31)

 $\forall t \in [t_0, \infty), \ \forall n$, where $n \in \mathbb{N}$ represents the nth iteration the crank enters/exits an FES region, and consequently, the nth iteration the crank enters/exits a KDZ, and $\Lambda \in \mathbb{R}_{>0}$ is defined as $\Lambda \triangleq (1/\overline{\lambda}) \min(\alpha, k_1)$, provided the following gain conditions are satisfied:

$$k_2 > c_1, \quad k_3 > c_2, \quad k_4 > c_3$$
 (32)

and $k_5 \ge B_{\overline{\sigma}}$ if $q \in \mathcal{Q}_{FES}$, $k_5 = 0$ if $q \in \mathcal{Q}_{KDZ}$, where c_1 , c_2 , c_3 , and $B_{\overline{\sigma}}$ are defined in (17)–(19), and Property 8, respectively.

Proof: Let z(t) be a Filippov solution to the differential inclusion $\dot{z} \in K[h_1](z)$, where $K[\cdot]$ is defined as in [37], and where $h_1 : \mathbb{R}^2 \to \mathbb{R}^2$ is defined using (15) and (26), as

 $h_1 \triangleq [\dot{e}_1 \ \dot{e}_2]^T$. The time derivative of (28) exists almost everywhere (a.e.) (i.e., for almost all $t \in [t_0, \infty)$), and $\dot{V}_1(z) \in \dot{V}_1(z)$, where \dot{V}_1 is the generalized time derivative of (28) along the Filippov trajectories of $\dot{z} = h_1(z)$ and is defined as [38] $\dot{V}_1 \triangleq \bigcap_{\bar{z} \in \partial V_1(z)} \zeta^T K[h_1(z) \ 1]^T$, where ∂V_1 is the Clarke generalized gradient of V_1 . Since V_1 is continuously differentiable in z, $\partial V_1 = \{\nabla V_1\}$; thus, $\dot{V}_1 \subseteq [e_1 \ Me_2 \ (1/2)\dot{M}e_2^2]K[h_1(z) \ 1]^T$. Using the calculus of $K[\cdot]$ from [38], substituting (15), (25), and (26) into the result yields

$$\dot{\tilde{V}}_{1} \subseteq -ae_{1}^{2} + e_{2}\chi_{1} + \left(\frac{1}{2}\dot{M} - V\right)e_{2}^{2} - k_{1}e_{2}^{2} \\
- (k_{2} + k_{3}\|z\| + k_{4}\|z\|^{2})K[\operatorname{sgn}(e_{2})]e_{2} \\
- \frac{k_{5}}{B_{\underline{\sigma}}}(k_{6}|e_{3}| + k_{7}K[|\operatorname{sgn}(e_{3})|])K[\operatorname{sgn}(e_{2})]e_{2} \\
- e_{2}\frac{K[B_{\underline{\sigma}}]}{B_{\underline{\sigma}}}(k_{6}e_{3} + k_{7}K[\operatorname{sgn}(e_{3})])$$
(33)

where $K[\operatorname{sgn}(\cdot)] = \operatorname{SGN}(\cdot)$ such that $\operatorname{SGN}(\cdot) = \{1\}$ if $(\cdot) > 0$, [-1, 1] if $(\cdot) = 0$, and $\{-1\}$ if $(\cdot) < 0$; and $K[|\operatorname{sgn}(\cdot)|] = |\operatorname{SGN}(\cdot)|$ such that $|\operatorname{SGN}(\cdot)| = \{1\}$ if $(\cdot) \neq 0$, and [0, 1] if $(\cdot) = 0$. To illustrate convergence for all time, the expression in (33) must be evaluated when $q \in \mathcal{Q}_{FES}$ and $q \in \mathcal{Q}_{KDZ}$.

For $q \in \mathcal{Q}_{FES}$, $K[B_{\sigma}]$ can be upper bounded by $B_{\overline{\sigma}}$, hence by Properties 7 and 8, and since $\dot{V}_1(z) \in \tilde{V}_1(z)$, (33) can be bounded as

$$\dot{V}_{1} \stackrel{\text{a.e.}}{\leq} -\alpha e_{1}^{2} + |e_{2}\chi_{1}| - k_{1}e_{2}^{2} - |e_{2}|(k_{2} + k_{3}||z|| + k_{4}||z||^{2}) \\
- \frac{(k_{5} - B_{\overline{\sigma}})}{B_{\sigma}} |e_{2}|(k_{6}|e_{3}| + k_{7}). \quad (34)$$

Using Properties 1-6 allows (34) to be further upper bounded as

$$\dot{V}_{1} \stackrel{\text{a.e.}}{\leq} -\alpha e_{1}^{2} - k_{1}e_{2}^{2} - \lambda_{1}|e_{2}| - \lambda_{2}|e_{2}| ||z||
- \lambda_{3}|e_{2}| ||z||^{2} - \frac{\lambda_{4}}{B_{\sigma}}|e_{2}|(k_{6}|e_{3}| + k_{7})$$
(35)

where $\lambda_i \in \mathbb{R}$, $\forall i \in \mathcal{I} = \{1, 2, 3, 4\}$ are known constants defined as $\lambda_1 \triangleq k_2 - c_1$, $\lambda_2 \triangleq k_3 - c_2$, $\lambda_3 \triangleq k_4 - c_3$, $\lambda_4 \triangleq k_5 - B_{\overline{\sigma}}$. By Property 8, (35) holds for all B_{σ} ; hence, (28) is verified as a common Lyapunov function across the controlled regions. Provided the gain conditions in (32) are satisfied, $\lambda_i \geq 0$, $\forall i \in \mathcal{I}$, and (35) can be upper bounded as

$$\dot{V}_1 \stackrel{\text{a.e.}}{\leq} -\Lambda V_1 \tag{36}$$

where Λ was previously defined. Solving the differential inequality yields

$$V_1 \le V_1(t_n^{\text{FES}}) \exp\left(-\Lambda(t - t_n^{\text{FES}})\right).$$
 (37)

When evaluating (33) for $q \in Q_{KDZ}$, Property 7, and the fact that $k_5 = 0$ if $q \in Q_{KDZ}$, allows (33) to be bounded as

$$\dot{V}_1 \stackrel{\text{a.e.}}{\leq} -\alpha e_1^2 + |e_2\chi_1| - k_1 e_2^2 - |e_2|(k_2 + k_3||z|| + k_4||z||^2). \tag{38}$$

Properties 1-6 allow (38) to be further upper bounded as

$$\dot{V}_1 \stackrel{\text{a.e.}}{\leq} -\alpha e_1^2 - k_1 e_2^2 - (\lambda_1 + \lambda_2 ||z|| + \lambda_3 ||z||^2) |e_2| \quad (39)$$

which can further be upper bounded as (36) provided the gain conditions in (32) are satisfied. Hence, (28) is a common Lyapunov function for all time. Based on (30) and (36), the result in (31) can be obtained, and from the closed-loop error systems, the controller in (24) is bounded. Hence, the first control objective is satisfied (i.e., cadence tracking).

Because incomplete control authority exists over the torque tracking objective (i.e., the rider's muscles are stimulated in the FES region, but not in the KDZ region), the following theorem is employed to establish a decay rate on the torque error system in the FES region and a growth rate in the KDZ region.

Theorem 2: For $q \in Q_{FES}$, the closed-loop error system in (27) yields exponential torque tracking in the sense that

$$|e_3(t)| \le |e_3(t_n^{\text{FES}})| \exp[-k_6(t - t_n^{\text{FES}})]$$
 (40)

 $\forall t \in [t_n^{\text{FES}}, t_n^{\text{KDZ}})$ and $\forall n$, where $t_n^{\text{FES}} \in \mathbb{R}_{\geq 0}$ is the time the crank enters Q_{FES} of cycle n, provided the gain conditions in (32) and the following constant gain condition is satisfied:

$$k_7 \ge c_4 \tag{41}$$

where c_4 was introduced in (23). In addition, for $q \in Q_{KDZ}$, the torque tracking error can be bounded as

$$|e_{3}(t)| \le \begin{cases} \sqrt{|e_{3}(t_{n}^{KDZ})|^{2} + c_{4}\sqrt{8}(t - t_{n}^{KDZ})}, & \text{for } |e_{3}| \le \sqrt{2} \\ |e_{3}(t_{n}^{KDZ})| \exp\left(\frac{c_{4}}{\sqrt{2}}(t - t_{n}^{KDZ})\right), & \text{for } |e_{3}| > \sqrt{2} \end{cases}$$
(42)

 $\forall t \in [t_n^{\text{KDZ}}, t_{n+1}^{\text{FES}})$, and $\forall n$, where $t_n^{\text{KDZ}} \in \mathbb{R}_{\geq 0}$ is the time the crank enters Q_{KDZ} (i.e., exits Q_{FES}) of cycle n.

Proof: Using a similar strategy to that employed in Theorem 1 for (27) yields

$$\dot{\tilde{V}}_2 \subseteq e_3 \chi_2 - \frac{B_{\sigma}}{B_{\sigma}} (k_6 e_3^2 + k_7 K[\text{sgn}(e_3)] e_3)$$
 (43)

where $K[B_{\sigma}] = B_{\sigma}$ within the FES regions. By Property 8, and since $\dot{V}_2(e_3) \stackrel{\text{a.c.}}{\in} \dot{V}_2(e_3)$, (43) can be bounded using Assumption 2 as

$$\dot{V}_2 \stackrel{\text{a.e.}}{\leq} -k_6 e_3^2 - \lambda_5 |e_3|$$
 (44)

where $\lambda_5 \in \mathbb{R}$ is a known constant defined as $\lambda_5 \triangleq k_7 - c_4$. By Property 8, (29) is verified as a common Lyapunov function across the controlled regions. Provided the gain condition in (41) is satisfied, (44) can be upper bounded as

$$\dot{V}_2 \stackrel{\text{a.e.}}{\leq} -2k_6V_2.$$
 (45)

Solving the differential inequality in (45) yields

$$V_2 \le V_2(t_n^{\text{FES}}) \exp(-2k_6(t - t_n^{\text{FES}})).$$
 (46)

Hence, by (29), the result in (40) can be obtained.

When $q \in Q_{KDZ}$, the control input term $k_5u_{tor} = 0$, and the expression in (43) can be written as

$$\dot{\tilde{V}}_2 \subseteq e_3 \chi_2 \tag{47}$$

because $B_{\sigma} = 0$. Using (29), and since $\dot{V}_2(e_3) \in \dot{V}_2(e_3)$, (47) can be upper bounded as

$$\dot{V}_2 \stackrel{\text{a.e.}}{\leq} c_4 \sqrt{2V_2}.$$
 (48)

From (48)

$$\dot{V}_2 \stackrel{\text{a.e.}}{\leq} \begin{cases} c_4 \sqrt{2}, & \text{if } V_2 \leq 1 \\ c_4 \sqrt{2} V_2, & \text{if } V_2 > 1 \end{cases}$$
 (49)

By invoking the Comparison Lemma [39, Lemma 3.4] for each

$$V_2 \le \begin{cases} V_2(t_n^{\text{KDZ}}) + c_4 \sqrt{2} (t - t_n^{\text{KDZ}}), & \text{if } V_2 \le 1 \\ V_2(t_n^{\text{KDZ}}) \exp\left(c_4 \sqrt{2} (t - t_n^{\text{KDZ}})\right), & \text{if } V_2 > 1 \end{cases}$$
 (50)

error systems, the controller in (25) is bounded.

Despite the growth of the torque error system in the KDZ region, the following theorem leverages the results of Theorem 2 to guarantee convergence to an ultimate bound through dwell-time conditions which manifest themselves as a minimum and maximum allowable cadence.

Theorem 3: For $q \in \mathcal{Q}$, the closed-loop error system in (27) yields a uniformly ultimately bounded torque tracking error in

$$|e_3(t)| \le 4\sqrt{\exp\left(-2k_6\Delta t_{\min}^{\text{FES}}\right) + c_4\sqrt{2}\Delta t_{\max}^{\text{KDZ}}} \le \sqrt{2}$$
 (51)

 $\forall t \in [t_0, \infty)$ when (41) and the following gain condition is satisfied:

$$k_6 \ge \max\left(\frac{c_4\sqrt{2}\Delta t_{\max}^{KDZ}}{2\Delta t_{\min}^{FES}}, \frac{\ln\left(1 - c_4\sqrt{2}\Delta t_{\max}^{KDZ}\right)}{2\Delta t_{\min}^{FES}}\right)$$

in addition to $\Delta t_{\text{max}}^{\text{KDZ}} < (1/c_4\sqrt{2})$, where $\Delta t_{\text{min}}^{\text{FES}}$, $\Delta t_{\text{max}}^{\text{KDZ}} \in \mathbb{R}_{>0}$ are known constants defined as

$$\Delta t_{\min}^{\text{FES}} \triangleq \min \left(t_n^{\text{KDZ}} - t_n^{\text{FES}} \right)$$
 (52)
 $\Delta t_{\max}^{\text{KDZ}} \triangleq \max \left(t_{n+1}^{\text{FES}} - t_n^{\text{KDZ}} \right)$ (53)

$$\Delta t_{\text{max}}^{\text{KDZ}} \triangleq \max \left(t_{n+1}^{\text{FES}} - t_n^{\text{KDZ}} \right)$$
 (53)

which denote the minimum allowable dwell-time in the FES region and the maximum allowable dwell-time in the KDZ region, $\forall n$, as dictated by the selectable minimum and maximum allowable cadences, respectively.

Proof: By evaluating V_2 at the switching instances (i.e., $V_2(t_n^{\text{FES}})$) and enforcing

$$V_2(t_{n+1}^{FES}) \le V_2(t_n^{FES})$$
 (54)

an ultimate bound is guaranteed to exist. Specifically, using (46) and (50), (54) can be rewritten as

$$V_{2}(t_{n+1}^{\text{FES}}) = \begin{cases} V_{2}(t_{n}^{\text{FES}}) \exp\left(-2k_{6}(t_{n}^{\text{KDZ}} - t_{n}^{\text{FES}})\right) \\ +c_{4}\sqrt{2}(t_{n+1}^{\text{FES}} - t_{n}^{\text{KDZ}}), & \text{if } V_{2} \leq 1 \\ V_{2}(t_{n}^{\text{FES}}) \exp\left(-2k_{6}(t_{n}^{\text{KDZ}} - t_{n}^{\text{FES}}) \\ +c_{4}\sqrt{2}(t_{n+1}^{\text{FES}} - t_{n}^{\text{KDZ}})\right), & \text{if } V_{2} > 1 \end{cases}$$
(55)

By examining the worst case scenario (i.e., inserting the minimum and maximum allowable dwell-times), (55) can be bounded as

$$V_{2}(t_{n+1}^{\text{FES}}) = \begin{cases} V_{2}(t_{n}^{\text{FES}}) \exp\left(-2k_{6}\Delta t_{\min}^{\text{FES}}\right) + c_{4}\sqrt{2}\Delta t_{\max}^{\text{KDZ}}, & \text{if } V_{2} \leq 1\\ V_{2}(t_{n}^{\text{FES}}) \exp\left(c_{4}\sqrt{2}\Delta t_{\max}^{\text{KDZ}} - 2k_{6}\Delta t_{\min}^{\text{FES}}\right), & \text{if } V_{2} > 1 \end{cases}$$
(56)

Examining (56), when $V_2 \le 1$, and inserting the largest possible initial condition [i.e., $V_2(t_n^{\text{FES}}) = 1$], (56) simplifies to

$$V_2(t_{n+1}^{\text{FES}}) \le \exp\left(-2k_6\Delta t_{\min}^{\text{FES}}\right) + c_4\sqrt{2}\Delta t_{\max}^{\text{KDZ}}.$$
 (57)

To enforce overall decay, $V_2(t_{n+1}^{\rm FES})$ needs to be less than the initial condition (i.e., $V_2(t_{n+1}^{\rm FES}) < 1$), and (57) becomes

$$1 \ge \exp\left(-2k_6\Delta t_{\min}^{\text{FES}}\right) + c_4\sqrt{2}\Delta t_{\max}^{\text{KDZ}}$$

which can be solved for the gain condition

$$k_6 \ge \frac{\ln\left(1 - c_4\sqrt{2}\Delta t_{\text{max}}^{\text{KDZ}}\right)}{2\Delta t_{\text{min}}^{\text{FES}}}.$$
 (58)

Hence, for $V_2 \le 1$, the ultimate bound is

$$V_2 \le \exp\left(-2k_6\Delta t_{\min}^{\text{FES}}\right) + c_4\sqrt{2}\Delta t_{\max}^{\text{KDZ}} \le 1.$$
 (59)

Examining (56) when $V_2 > 1$ and imposing the following gain condition will result in overall exponential decay to the smallest possible bound (i.e., $\lim_{t\to\infty} V_2 = 1$)

$$k_6 \ge \frac{c_4 \sqrt{2} \Delta t_{\text{max}}^{\text{KDZ}}}{2 \Delta t_{\text{min}}^{\text{FES}}}.$$
 (60)

Because overall decay is enforced for both the above conditions (i.e., $V_2 \le 1$ and $V_2 > 1$), the overall ultimate bound is given by (59) provided the gain conditions in (58) and (60) are satisfied. Fig. 3 provides an example decay to the ultimate bound using (46) and (50). Bounding (59) with (29) provides the result in (51).

Where Theorem 3 establishes an ultimate bound for the integral torque tracking error (i.e., e_3), Theorem 4 provides a bound on the instantaneous torque tracking error (i.e., \dot{e}_3).

Theorem 4: For $q \in Q$, the closed-loop error system in (27) yields a uniformly ultimately bounded instantaneous torque tracking error in the sense that

$$|\dot{e}_{3}| \stackrel{\text{a.e.}}{\leq} c_{4} + \frac{B_{\overline{\sigma}}}{B_{\underline{\sigma}}} (k_{7} + 4k_{6} \cdot \sqrt{\exp\left(-2k_{6}\Delta t_{\min}^{\text{FES}}\right)} + c_{4}\sqrt{2}\Delta t_{\max}^{\text{KDZ}}).$$
(61)

Proof: To establish an ultimate bound on \dot{e}_3 , the result in (43) is evaluated for $q \in Q_{FES}$ and $q \in Q_{KDZ}$ as

$$\dot{\bar{V}}_2 \subseteq \begin{cases} e_3 \chi_2 - \frac{B_{\sigma}}{B_{\underline{\sigma}}} (k_6 e_3^2 + k_7 K [\operatorname{sgn}(e_3)] e_3), & \text{if } q \in \mathcal{Q}_{\text{FES}} \\ e_3 \chi_2, & \text{if } q \in \mathcal{Q}_{\text{KDZ}} \end{cases}.$$
(62)

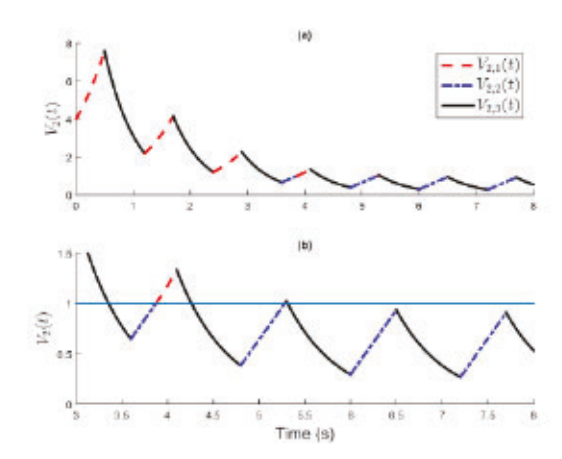


Fig. 3. (a) Sample Lyapunov function evolution over n=8 cycles with parameters $V_2(t_0)=4$, $c_4\sqrt{2}=1.28$, $k_6=3.56$, $\Delta t^{\rm KDZ}=0.5$ s, $\Delta t^{\rm FES}=0.7$ s (i.e., constant 50 RPM with the FES regions representing 58% of the crank cycle and KDZs representing 42%). The Lyapunov function $V_{2,1}$ represents the exponential growth bound for $V_2>1$ in the KDZ, $V_{2,2}$ represents the linear growth bound for $V_2\le 1$ in the KDZ, and $V_{2,3}$ represents the exponential decay bound in the FES regions. (b) Same sequence of Lyapunov functions, with an emphasis on the ultimate bound being less than 1, obtained by adhering to the gain conditions in (58) and (60).

Using (29), and since $\dot{V}_2(e_3) \stackrel{\text{a.e.}}{\in} \dot{\tilde{V}}_2(e_3)$, (62) can be rewritten as

$$\dot{e}_{3} \stackrel{\text{a.e.}}{=} \begin{cases} \chi_{2} - \frac{B_{\sigma}}{B_{\underline{\sigma}}} (k_{6}e_{3} + k_{7}K[\operatorname{sgn}(e_{3})]), & \text{if } q \in \mathcal{Q}_{\text{FES}} \\ \chi_{2}, & \text{if } q \in \mathcal{Q}_{\text{KDZ}}. \end{cases}$$
(63)

Establishing the most aggressive decay and growth rate for the FES and KDZ regions, respectively, will provide an ultimate bound on \dot{e}_3 . For $q \in Q_{FES}$, (63) must be lower bounded. Using Property 8, and bounding yields

$$\dot{e}_3 \stackrel{\text{a.e.}}{\geq} -c_4 - \frac{B_{\bar{\sigma}}}{B_{\sigma}} (k_6 |e_3| + k_7).$$
 (64)

For $q \in \mathcal{Q}_{KDZ}$, (63) must be upper bounded, which when combined with (23) yields the most aggressive growth rate in the KDZ regions given by

$$\dot{e}_3 \stackrel{\text{a.c.}}{\leq} c_4. \tag{65}$$

After combining the bounds in both the FES and KDZ regions [i.e., (64) and (65)] with the ultimate bound on e_3 given in (51), the maximum absolute value of the two is taken to obtain the ultimate bound on \dot{e}_3 in (61).

V. EXPERIMENTS

Experiments were conducted to validate the performance of the developed controller, henceforth labeled Controller A, in both an able-bodied population and a population with varied NCs. To further examine the performance compared to alternate methods of cadence and power control, two other controllers were implemented, labeled Controller B and Controller C, whose development and stability analyses are available in [29] and [30], respectively. While the forms of the three controllers are different, all have the same objective of

TABLE I CONTROLLER OPERATIONAL DETAILS

Controller	Region	Motor Objective	Muscle Objective	
A	FES	Cadence	Instantaneous Pow	
A	KDZ	Cadence	None	
B [29]	FES	Instantaneous Power	Cadence	
D [29]	KDZ	Cadence	None	
C [20]	FES	Cadence	Discretized Powe	
C [30]	KDZ	Cadence	None	

cadence and power tracking. Although the tracking objectives in the FES regions vary, all three controllers utilize the motor to track cadence in the KDZ regions because no muscles are activated; see Table I for details.

Although the error systems and controllers take different forms, a side-by-side comparison is made because all controllers possess the same desired cadence and power trajectories for a given participant. By comparing the three controllers, insights are provided to determine which actuator (i.e., muscle or motor) results in better tracking performance of the objectives (i.e., cadence or power) and which is the better method to track power (i.e., instantaneously or discretely).

A. Experimental Testbed

The experimental testbed consisted of a stationary Terra-Trike Rover recumbent tricycle mounted on a Kinetic Bike Trainer. A 250-W, 24-V dc brushed motor, by Unite Motor Co. Ltd., was mounted under the frame of the cycle and was coupled to the drive chain to allow for motor assistance/resistance. The motor was interfaced with an ADVANCED Motion Controls5 (AMC) PS300W24 power supply and an AMC AB25A100 motor driver. An AMC FC15030 filter card was wired between the motor and power supply to reduce electrical noise. The crank angle was measured using a US Digital H5 optical encoder coupled to the crank through gears. Brackets attached to commercially available bike pedals allowed for the mounting of orthotic boots which fix the rider's feet to the pedals and prevent dorsiflexion and plantarflexion of the ankles, maintaining sagittal alignment of the legs. Torque applied about the crank was measured using an SRM Science Road Wireless Powermeter mounted to the bike crank. A Quanser Q8-USB DAQ was used to interface with the encoders, motor driver, and powermeter. Controllers were implemented on a computer using MATLAB/Simulink, Quarc, and Windows 7 at a sample rate of 500 Hz. A Hasomed Rehastim 1 current-controlled stimulator delivered biphasic, symmetric, rectangular pulses to the participant's muscle groups via bipolar, self-adhesive, PALS® electrodes.6 The stimulation was applied at 60 Hz and amplitudes were fixed at 90, 80, and 70 mA for the quadriceps, hamstrings, and gluteals, respectively. The stimulation pulsewidth for each muscle group was determined by the controller and commanded to the

stimulator by the control software. An emergency stop button was fastened to the tricycle that enabled the participant to immediately stop the experiment if desired.

B. Experimental Methods

Seven able-bodied participants (five male and two female) with ages ranging from 21 to 43 years old, and six participants with NCs (four male and two female) with ages ranging from 20 to 48 years old participated in the experimental protocol. Participants were either recruited through the University of Florida (UF) Health Integrated Data Repository (UF Consent2Share project) and completed the FES-cycling protocol at UF or were enrolled at Brooks Rehabilitation Hospital in Jacksonville, FL. All participants gave written informed consent approved by the UF Institutional Review Board. Able-bodied participants were blind to the desired trajectories, and asked to remain passive for the duration of the experiment unless otherwise noted. Removing volitional contribution simulates a worst case scenario where the participant's muscles provide no contribution to the trajectory. Although some volitional contribution is still possible and not measured, any voluntary contribution was only partially informed by stimulation cues because participants were unaware of the desired trajectories. Similar to active therapy, participants with a NC were asked to volitionally pedal with stimulation added as needed. These participants were shown a graph of the tracking performance of e_3 , exclusively, and asked to contribute to the control objective to the greatest extent possible. In the able-bodied population, all three controllers were implemented in random order. In the population possessing neurological disorders, Controllers A and C were implemented in the random order.

In preparation for experimentation, electrodes were placed on the quadriceps femoris, hamstrings, and gluteal muscle groups of a person who was seated with their feet inserted securely into the orthotic pedals attached to the cycle. The tricycle's seat position was adjusted for the person's comfort while ensuring that full extension of the knees could not be achieved (i.e., maintaining a minimum bend of 15° at the knee) while cycling. Measurements including the person's thigh and shank length, as well as distance from the person's greater trochanter to the crank in both the horizontal and vertical directions, were made to calculate the torque transfer ratios and determine the stimulation pattern based on Q_m . Prior to stimulation, the participant's range of motion and comfort was verified by running the cycle at 30, 40, and 50 RPM, sequentially. Upon reaching 50 RPM, open-loop stimulation was applied and modulated until muscle contractions were visible. For comfort, if the person's threshold was reached during calibration, the stimulation value was saved by the controller and the stimulation was saturated at this level for the duration of the experiment.

The estimate of the rider's passive dynamics, $\hat{\tau}_{est}$, was generated by simultaneously running the cycle at the desired cadence (50 RPM) while recording the torque from the powermeter; the rider was instructed to provide no volitional effort. Subsequently, an eighth-order Fourier fit was applied to the recorded torque measurements to satisfy Assumption 2.

⁵ADVANCED Motion Controls supported the development of this testbed by providing discounts on their branded items.

⁶Surface electrodes for this study were provided compliments of Axelgaard Manufacturing Co., Ltd.

Afterward, a 180-s experimental protocol was performed on the participant, which began with an exponential ramp to the desired cadence using only the motor. Upon reaching the desired cadence, the power trajectory then began increasing along an exponential ramp until the desired power was obtained, at which point stimulation was applied. The cadence controller given in (24) was active during and after the cadence ramp, where the torque controller given in (25) was only active after the desired cadence had been reached because large muscle forces are required to move the crank at low speeds [14]. While there is no clear consensus for the optimal cadence of FES cycles for rehabilitation, it has been suggested that lower cadences may be more ideal for torque production, while higher cadences may be better for power production [14]. However, for feasibility purposes, the desired cadence was set to 50 RPM [20], [40] for both the able-bodied population and the population with neurological impairments, without loss of generality.

The desired power is denoted by $P_d: \mathbb{R}_{\geq 0} \to \mathbb{R}$ and defined as the product of the desired torque and desired cadence (i.e., $P_d \triangleq \tau_{m,d}\dot{q}_d$), and varied based on participant capability. For feasibility purposes, the desired power trajectory was held constant after an initial ramp to the desired value. However, in practice, the desired power can be time-varying as long as it remains continuously differentiable and the estimate of the rider's passive dynamics are collected over the same trajectory.

Although the muscles are stimulated with the controller in (25) utilizing a torque-based error system, the following results are displayed in terms of measured power, denoted by $P: \mathbb{R}_{\geq 0} \to \mathbb{R}$, defined as the product of the estimated rider torque and measured cadence (i.e., $P \triangleq \hat{\tau}_m \dot{q}$).

To account for the unmodeled dynamics present in the rider's muscles, the stimulation pattern was empirically corrected and advanced as a function of the cadence (i.e., $q_{\text{stim}} \triangleq q + 0.1\dot{q}$), where $q_{\text{stim}}: \mathcal{Q} \times \mathbb{R} \to \mathcal{Q}$ was substituted for q in (4). Although the aforementioned gain conditions (i.e., $k_2 \ge c_1$, $k_3 \ge c_2$, $k_4 \ge c_3$, $k_5 \ge B_{\sigma}$, $k_6 \ge$ $\max((c_4\sqrt{2}\Delta t_{\max}^{\text{KDZ}}/2\Delta t_{\min}^{\text{FES}}), (\ln(1-c_4\sqrt{2}\Delta t_{\max}^{\text{KDZ}})/2\Delta t_{\min}^{\text{FES}})),$ $k_7 \ge c_4$ in (32), (41), (58), and (60)) are sufficient to achieve stability for the largest uncertainties on the system parameters, they represent conservative gains required by the controllers in (24) and (25). Therefore, the gain conditions provide guidelines and bounds for the initial gain selection and the gains can be subsequently adjusted to achieve desirable performance as part of the experiment. The listed gains were adjusted using an empirical-based method, but the gains could have been adjusted using more methodical approaches. For example, the nonlinear system in [41] was linearized at several operating points and a linear controller was designed for each point, and the gains were chosen by interpolating, or scheduling the linear controllers. In [42], a neural network is used to tune the gains of a proportional—integral—differential (PID) controller. In [43], a genetic algorithm was used to fine tune the gains after initialization and guesses were made by the controller designer. Killingsworth and Krstic [44] provide an extensive discussion on the use of extremum seeking for tuning the gains of a PID controller. In addition, in [45], the tuning of a PID controller for robot manipulators is discussed.

TABLE II

COMPARATIVE RESULTS FOR ABLE-BODIED POPULATION: MEAN ERROR
OF TRACKING OBJECTIVES GIVEN AS $\dot{\bar{e}} \pm \text{STD}(\dot{e})$, AND
PERCENT ERROR OF $\dot{\bar{e}}$ DURING STEADY-STATE
OPERATION FOR CADENCE AND POWER*

Controller	Participant	ē₁ (RPM)	(% Error)	$\overline{\dot{e}_3}/\overline{e_{\tau}} \; (\mathrm{W})^{\dagger,\ddagger}$	$\frac{\overline{e}_3}{\overline{e}_{\tau}}$ (% Error)
	A	0.01±0.88	0.02	-0.08±0.33	0.76
	В	0.03±0.72	0.05	-0.04±0.38	0.38
	С	0.01±0.70	0.03	-0.00±0.50	0.02
	D	0.02±0.93	0.03	-0.05±0.69	0.48
^	E	0.01 ± 1.03	0.03	0.01 ± 0.70	0.06
	F (6W)	0.02±0.99	0.04	0.16±0.69	2.60
	G (15W)#	0.00±1.65	0.00	0.02 ± 2.05	0.11
	Average	0.01±1.03	0.03	0.00±0.94	0.63
	A	-0.19±5.38	0.39	-0.03±1.48	0.28
	В	-0.15±5.46	0.30	-0.05±1.43	0.51
	C	-0.04±4.84	0.07	-0.02±1.46	0.18
В	D	-0.03±5.24	0.05	0.07±1.47	0.68
ь	Е	-0.10±6.16	0.19	-0.03±2.76	0.30
	F (6W)	-0.11±4.90	0.21	-0.02±1.26	0.32
	G (15W) ^Δ				
	Average	-0.10±5.35	0.21	-0.01±1.72	0.38
9	A	0.01±1.10	0.01	-0.10±0.69	1.00
	В	0.02±0.90	0.04	-0.10±0.76	0.99
	C	0.00±0.66	0.00	-0.30±0.98	0.27
C	D	0.03±0.96	0.06	0.02 ± 1.70	0.24
C	E	0.00±1.21	0.00	-0.21±1.50	2.13
	F (6W)	0.02±0.89	0.04	-0.00±0.74	0.01
	G (15W)#	0.02±0.90	0.04	0.24±3.54	1.61
	Average	0.01±0.96	0.03	-0.06±1.70	0.89

*Unless otherwise noted, all participants provided no volitional contribution; the desired cadence and power are 50 RPM and 10 W, respectively.

[†]The notation \dot{e}_3 is valid for the error systems of Controllers A and B. For Controller C in [30], it is analogous to $e_{\tau}(k)$, which represents the average torque error $e_{\tau}: \mathbb{N} \to \mathbb{R}$ per crank cycle, k.

[‡]For post-processing, a two crank cycle (a moving window of approximately 2.4 seconds) averaging filter was applied on \dot{e}_3/e_τ .

Due to participant comfort, this trial ended at two minutes.

#The participant provided volitional contribution.

△Due to time constraints by the participant, this experiment was not performed, and therefore, this participant was excluded from the statistical analysis.

For Controller A, the controller gains in (15), (24), and (25) were selected as $k_1 \in [5, 9]$, $k_2 \in [0.08, 0.10]$, $k_3 \in [0.02, 0.05]$, $k_4 \in [0.02, 0.05]$, $k_5 = 0.01$, $k_6 \in [15, 60]$, $k_7 \in [0.75, 4.0]$, $\alpha = 6$; for Controller B in [29], the controller gains were selected as $k_1 = 0.75$, $k_2 = 0.1$, $k_3 = 0.05$, $k_4 = 0.05$, $k_5 = 1.5$, $k_6 = 0.85$, $k_7 = 0.35$, $\alpha = 6$; and for Controller C in [30], the controller gains were selected as $k_1 = 15$, $k_2 = 1.5$, $k_3 = 7.5$, $k_4 \in [35, 50]$, $k_5 = 6$, $k_6 \in [30, 35]$, $\alpha \in [1, 6]$ across all trials.

C. Results From Able-Bodied Population

To validate the proposed controller, experiments were conducting using Controllers A, B, and C on able-bodied participants. The able-bodied population's cadence and power results are displayed in Table II; each controller was implemented on each participant for a single trial.

The developed controller (i.e., Controller A) demonstrated average cadence and power tracking errors of 0.01±1.03 RPM and 0.00±0.94 W, respectively; Controller B demonstrated average cadence and power tracking errors of

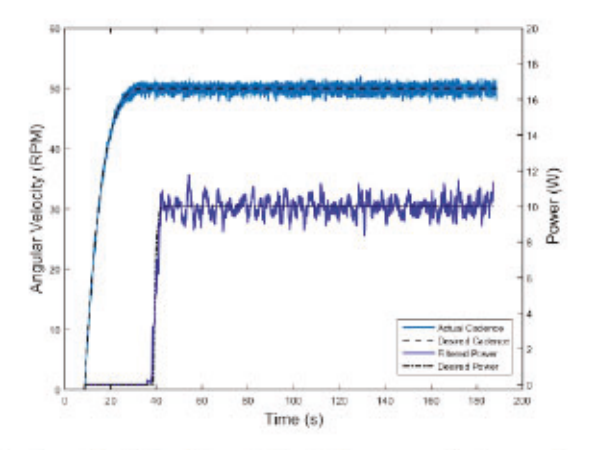


Fig. 4. Controller A, Participant C: Desired versus actual cadence and power. The mean cadence is 50.01±0.70 RPM and mean power is 10.00±0.50 W.

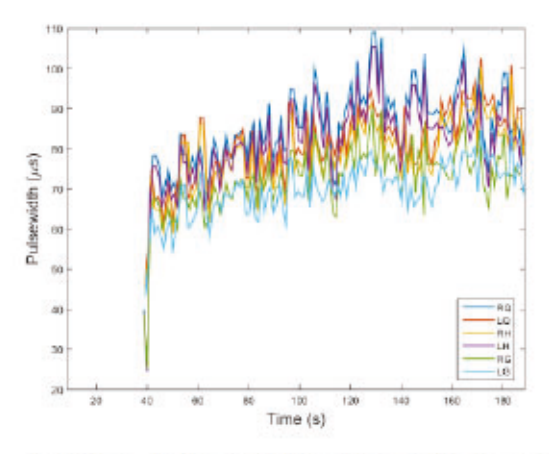


Fig. 5. Controller A, Participant C: Stimulation input to the participant's six muscle groups. Muscle groups are indicated by RQ, LQ, RH, LH, RG, LG, which represent right and left quadriceps, right and left hamstrings, and right and left gluteals, respectively. Although the stimulation input is activated/deactivated based on the switching signal in (4), the stimulation input is displayed as the maximum stimulation for each muscle group in each FES region, at the corresponding time.

-0.10±5.35 RPM and -0.01±1.72 W, respectively; and Controller C demonstrated average cadence and power tracking errors of 0.01±0.96 RPM and -0.06±1.70 W, respectively. For Participant C (as a typical result), plots of Controller A's cadence and power performance, and stimulation input are provided in Figs. 4-6; plots of Controller B's cadence and power performance, and stimulation inputs are provided in Figs. 7 and 8, respectively; and plots of Controller C's cadence and power performance, and stimulation inputs are provided in Figs. 9 and 10, respectively. To compare the current sent to the cycle's motor for each controller, Fig. 11 displays the motor control input for Controllers A, B, and C. For Participant C, compared to Controller C, Controller A drew 27% more current on average and Controller B drew 58% more current on average.

 Statistical Analysis and Discussion: To determine if the controller significantly affected the results, a Friedman test was conducted on the average cadence error, cadence standard deviations, average power error, and power standard deviations of Controllers A, B, and C. The Friedman test

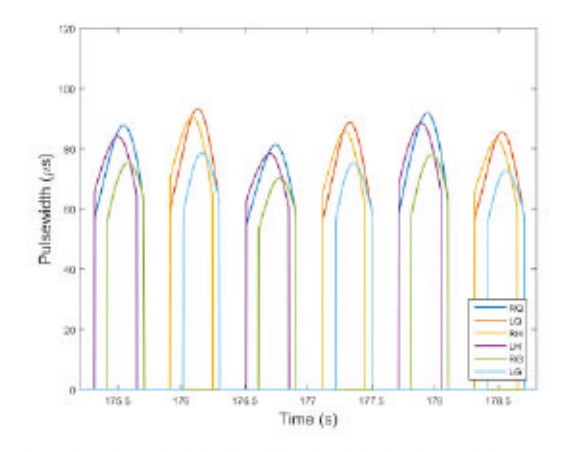


Fig. 6. Controller A, Participant C: Stimulation input for three revolutions.

used only the data from the participants who were used for all three controllers. Post-hoc comparisons between the three controllers were developed using Fisher's least significant difference (LSD) method to determine statistical significant differences. The first Friedman test was performed on the average cadence error, \dot{e}_1 , and determined that the choice of controller significantly affected the error (P = 0.0062). From the posttest, it was determined that Controller A was significantly different from Controller B (P = 0.0026), as was Controller B from C (P = 0.0159). Noting the average cadence errors in Table II, it is then concluded that Controllers A and C are both significantly superior than Controller B, but not from each other. The second Friedman test was conducted on the cadence standard deviations, $STD(\dot{e}_1)$, and indicated that the controller significantly affected the result (P = 0.0094). The posttest determined that Controllers A and B are significantly different (P = 0.0039) and so are Controllers B and C (P = 0.0209), with Controllers A and C superior to B. The third Friedman test was run on the average power errors, \dot{e}_3 , and indicated that the choice of controller did not significantly affect the result (P = 0.1146). However, the posttest found only Controllers A and C were significantly different (P = 0.0433) from each other, with A being superior. The final Friedman test, ran on the power standard deviations, STD(\dot{e}_3), again determined significant differences among the controllers (P = 0.0057). The posttest determined Controllers A and B were significantly different (P = 0.0015) and Controllers A and C were significantly different (P = 0.0433), with Controller A being superior in both cases. Hence, experimental results from the able-bodied population, indicate that Controllers A and C outperform B in both cadence and power tracking. These results indicate that the motor should control cadence for all time and the muscles should track power in the FES regions. Having the motor control cadence resulted in a reduction in the cadence standard deviation and a more comfortable participant experience due to less oscillatory pedaling performance.

Regardless of the controller, Figs. 4, 7, and 9 indicate that the measured cadence and power values fluctuate around the desired values throughout the experiment. The cause of these fluctuations can arise from system disturbances such

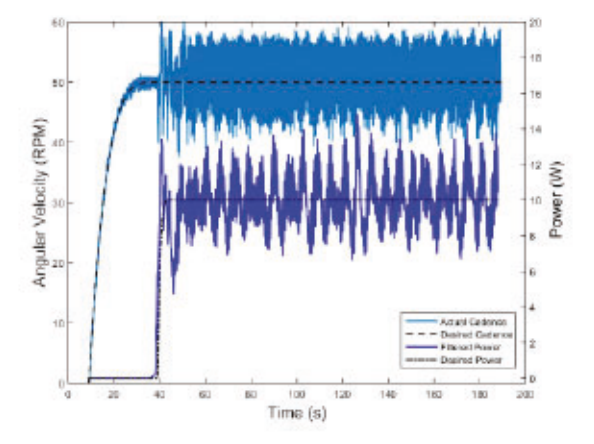


Fig. 7. Controller B, Participant C: Desired versus actual cadence and power. The mean cadence is 49.96±4.84 RPM and mean power is 9.98±1.46 W.

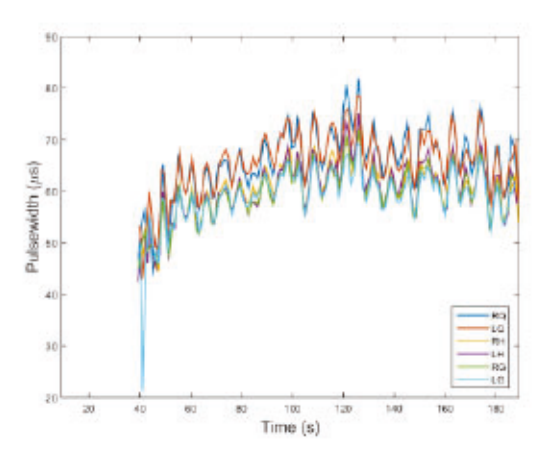


Fig. 8. Controller B, Participant C: Stimulation input to the participant's six muscle groups.

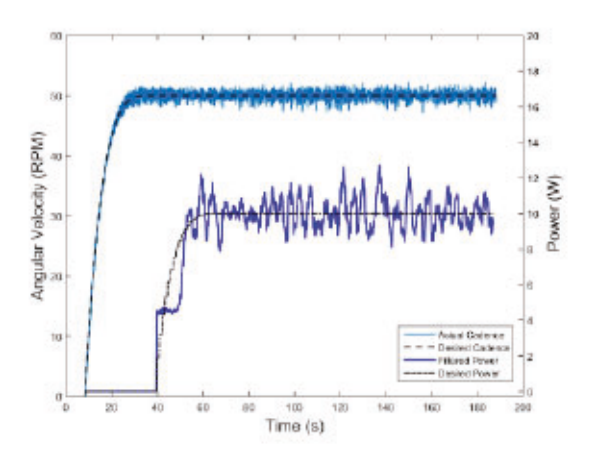


Fig. 9. Controller C, Participant C: Desired versus actual cadence and power. The mean cadence is 50.00±0.66 RPM and mean power is 9.70±0.98 W.

as chain links, the rider, or inaccurate modeling. Because each controller is designed to account for these disturbances, when the disturbance occurs, the controller is capable of compensating for it and correcting the measured trajectory. The degree of these fluctuations can be quantified using the standard deviation of cadence, displayed in Table II.

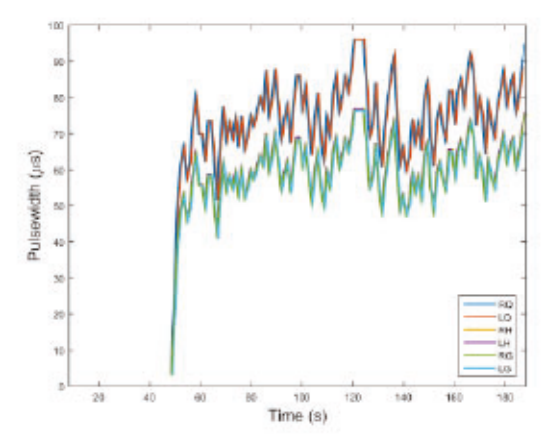


Fig. 10. Controller C, Participant C: Stimulation input to the participant's six muscle groups. Stimulation is identical for the right and left leg.

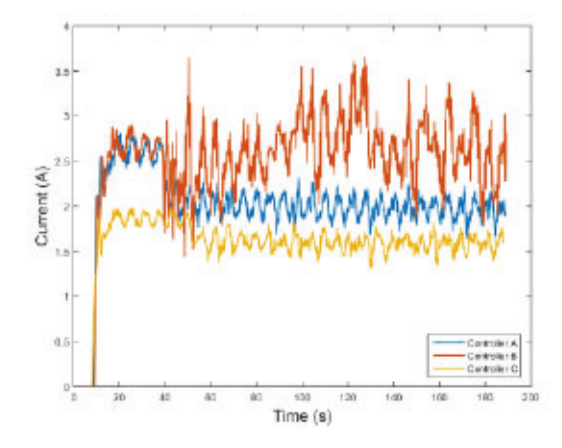


Fig. 11. Controllers A, B, and C, Participant C: Current input to the cycle's electric motor, filtered with a 1.2 s moving average for visual clarity.

Across all trials, the participant begins to show signs of fatigue, evidenced by the increasing amount of stimulation required to complete the tracking objective (see Figs. 5, 8, and 10). Because FES nonselectively recruits muscle fibers, closed-loop control offers one solution to compensate for the effect of fatigue. To reduce fatigue, the developed controller could have been implemented using [46], but compensating for fatigue remains an outstanding challenge in the use of FES [33]. Similarly, while results such as [47]–[49] offer inroads to compensating for neuromuscular delays, including such methods in more complex switched systems required for coordinating limb movements also remains an open challenge.

D. Results From Neurologically Impaired Population

Since Controllers A and C had comparable performance on the control population and superior performance over Controller B, only they were implemented on the population with neurological impairments to draw further conclusions. The population with neurological impairments is labeled numerically. These participants possess NCs such as hemorrhagic and ischemic stroke, SCI, spina bifida, and TBI. They also had varying degrees of exposure to FES; those who had prior

TABLE III
DEMOGRAPHICS OF POPULATION WITH NEUROLOGICAL IMPAIRMENTS

Participant	Age	Sex	Injury*	Active in FES	Active in PT/OT	Physical Aid [‡]	TSI [†]
1	45	M	Ischemic Stroke (L)	Y	Y	AFO	3yr 9mo
2	48	F	Hemorrhagic Stroke (L)	N	Y	AFO, Cane	9mo
3	20	M	SCI T8-9 Complete, T9-10 Fusion (AIS A)	Y	Y	Wheelchair	8mo
4	25	M	Spina Bifida (L5-S1), Arnold Chiari Malformation	Y	Y	AFO, Wheelchair	25yr
5	37	M	Traumatic Brain Injury	N	Y	AFO, Wheelchair	9yr 11mo
6	29	F	Ischemic Stroke (R)	N	Y	Wheelchair	1mo

^{*}L = Left Hemiparesis, R = Right Hemiparesis

^{*}AFO = Ankle Foot Orthosis



Fig. 12. Participant 4 seated on the motorized recumbent FES cycle. Label A indicates the encoder, label B indicates the powermeter, label C indicates the electrodes, label D indicates the emergency-stop, label E indicates the filter card, and label F indicates the stimulator. The electric motor is coupled to the drive chain below the seat.

experience were typically quicker to acclimate to the stimulation and had higher stimulation thresholds. To evaluate a participant's level of activity (i.e., how often they regularly perform exercise) and capabilities, they were asked to self-report if they regularly participate in physical or occupational therapy (PT/OT) and if they used any physical aid in ambulation. The participants' self-reported demographics are provided in Table III. Of the six participants, three suffered a stroke, all of which had hypersensitivity to electrical stimulation due to hemiparesis, resulting in lower stimulation thresholds. Stroke participants also had asymmetric motor impairments which, to varying degrees, affected limb coordination. Participant 3 lacks any sensation below the injury location and was unable to volitionally contribute to the task due to an SCI (AIS A). Controller A was implemented on all six participants and Controller C was implemented on five of the six. By performing experiments on participants with diverse neuromuscular conditions, the controller demonstrates stable tracking for a range of rider capabilities. Participant 4 seated on the FES cycle is shown in Fig. 12, and the experimental results are displayed in Table IV.

Controller A demonstrated average cadence and power tracking errors of 0.02±1.87 RPM and 0.00±2.46 W, respectively, and Controller C demonstrated average cadence and power tracking errors of 0.01±1.82 RPM and -0.54±3.96 W, respectively. To highlight the efficacy of the designed con-

TABLE IV

COMPARATIVE TRACKING RESULTS FOR POPULATION WITH NEUROLOGICAL IMPAIRMENTS: AVERAGE ERROR OF TRACKING OBJECTIVES GIVEN AS $\tilde{e} \pm \text{STD}(\hat{e})$, AND PERCENT ERROR OF \tilde{e} DURING STEADY STATE OPERATION FOR CADENCE AND POWER*

Controller	Participant	$\overline{\dot{e}_1}$ (RPM)	<u>έ</u> 1 (% Εποι)	$\overline{\dot{e}_3}/\overline{e_\tau} \ (\mathrm{W})^{\dagger,\ddagger}$	(% Error)
A	1 (8W)	0.01±1.69	0.03	0.09±3.08	1.11
	2 (10W)	0.02±1.85	0.05	-0.18±2.80	1.78
	3 (10W)	0.02±2.35	0.04	-0.02±0.52	0.16
	4 (5W)#	0.03±0.66	0.05	-0.24±0.50	4.76
	4 (5W)	0.01±0.56	0.02	0.01±0.41	0.21
	5 (10W)	0.02±1.50	0.05	0.29±4.12	2.90
	6 (5W)#	0.02±1.54	0.03	0.02±2.72	0.40
	Average	0.02±1.87	0.04	0.00±2.46	1.47
	1 (8W)	0.02±1.69	0.04	-2.31±3.61	-28.91
	2 (10W)	0.01±1.68	0.02	-0.81±3.10	-8.05
c	3 (10W)	0.02±2.79	0.05	-0.20±0.74	-2.01
C	4 (5W)	0.00±0.73	0.00	0.02 ± 0.19	0.36
	5 (10W)	0.01±1.59	0.02	0.58±7.44	5.81
	Combined	0.01±1.82	0.03	-0.54±3.96	9.03

*Unless otherwise noted, all participants provided volitional contribution; the desired cadence and power are 50 RPM and 10 W, respectively.

[†]The notation ė₃ is valid for the error systems of Controllers A and B. For Controller C in [30], it is analogous to e_T.

trollers, Participant 3's results are displayed in Figs. 13–16. Participant 3's results are depicted because he is paraplegic and unable to volitionally contribute to the forward motion of the crank; hence, any torque produced by the leg muscles is only caused by the controllers. Using Controller A, plots of his cadence and power performance and stimulation input are provided in Figs. 13 and 14. Using Controller C, plots of his cadence and power performance and stimulation input are provided in Figs. 15 and 16, respectively. To compare the current sent to the cycle's motor for each controller, Fig. 17 displays the motor control input for Controllers A and C. For Participant 3, Controller A drew an average of 33% more current than Controller C.

Statistical Analysis and Discussion: Although the participants with neurological impairments all possessed unique conditions, the following statistical analysis is provided to compare the controllers' ability to evoke desired behavior from the cycle and rider. By analyzing the controllers and their

[†]Time since injury (TSI)

 $^{^{\}ddagger}$ A two crank cycle filter was applied on \dot{e}_3/e_{τ} .

Participant did not provide any volitional contribution.

[#]Due to time constraints by the participant, the Controller C counterpart was not run, therefore this result was excluded from the signed-rank test.

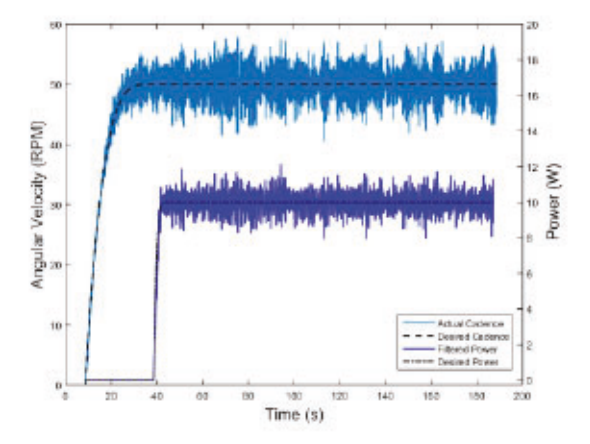


Fig. 13. Controller A, Participant 3: Desired versus actual cadence and power. The mean cadence is 50.02±2.35 RPM and mean power is 9.98±0.52 W.

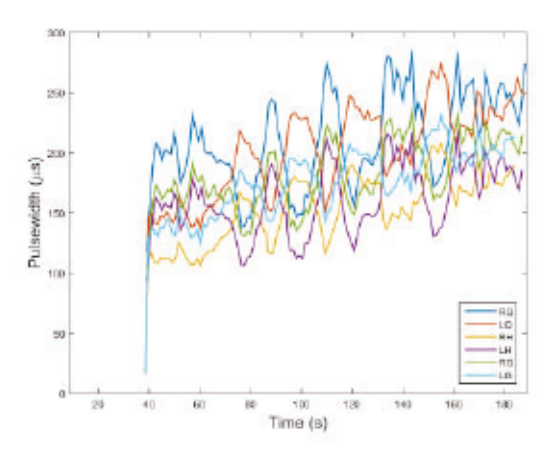


Fig. 14. Controller A, Participant 3: Stimulation input to the participant's six muscle groups.

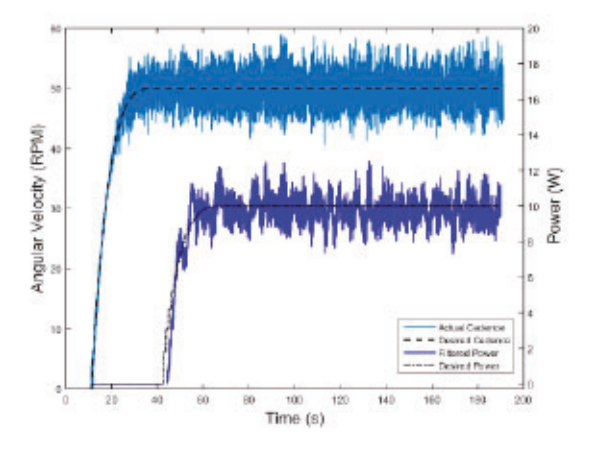


Fig. 15. Controller C, Participant 3: Desired versus actual cadence and power. The mean cadence is 50.02±2.79 RPM and mean power is 9.80±0.74 W.

respective tracking results, arguments are made which can potentially improve rehabilitation options across a spectrum of capabilities. While the cadence error and standard deviation are comparable for the two controllers, the average power error and standard deviation are smaller for Controller A than Controller C, though not statistically significant, i.e., $\alpha = 0.05$ (using the available paired data sets, i.e., Participants 1–5). It should be noted, however, because Controller C tracks power

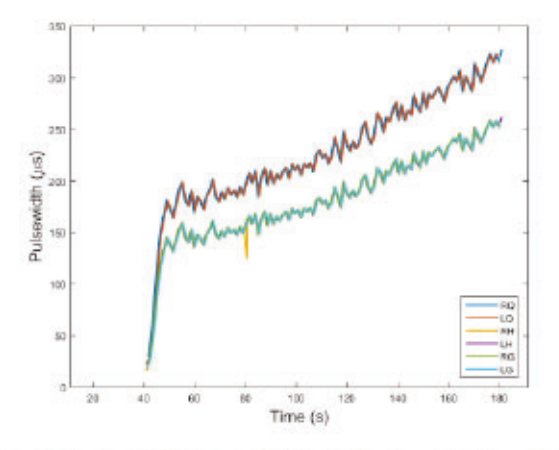


Fig. 16. Controller C, Participant 3: Stimulation input to the participant's six muscle groups.

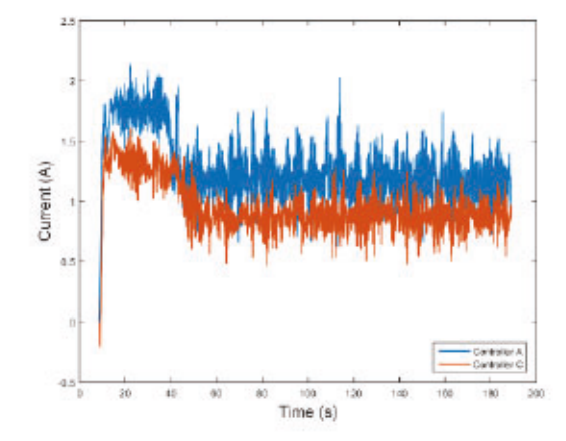


Fig. 17. Control Inputs, Participant C: Current input delivered to the cycle's electric motor for Controllers A and C, filtered with a 1.2 s moving average for visual clarity.

discretely, it potentially masks asymmetries in the rider. That is, because it updates the error and control input only once per cycle, Controller C delivers identical stimulation to both the right and left legs. Controller A uses a running integral to track power, updates continuously, and can potentially better accommodate asymmetries. As in the able-bodied population, the measured cadence and power values fluctuated around the desired values due to unmodeled disturbances, shown in Figs. 13 and 15. Future tests on a split-crank cycle could further explore differences for such asymmetries. Controller A outperformed C in terms of power tracking and power standard deviation but had a larger cadence standard deviation. Accounting for the errors, standard deviations, and potential masking of asymmetric characteristics, it is determined that Controller A should be used for the population with neurological impairments, and power should be tracked instantaneously, not discretely.

Controllers A and C were able to achieve power results comparable to those reported in other experiments involving people with SCIs (e.g., an average PO of 8.0±2.1 W with one leg at 25 RPM [8], an average steady state PO of 16.0±3.6 W ranged 8.5-29.5 W in five participants after one year of training [11], and an improvement from 8.4±1.0 W to 18.4±2.6 W in 11 participants after one year of training [12]).

VI. CONCLUSION

In this article, an FES cycling controller is developed to track both cadence and instantaneous torque. The torque error system uses a running integral to update the torque error in real-time, compared to once per cycle in discretized tracking prevalent in other cycling methods. Using the proposed controller, a Lyapunov-like switched system stability analysis is conducted which guarantees global exponential cadence tracking and uniform ultimate boundedness of the power objective. Experiments were conducted on seven able-bodied participants and six participants with neurological impairments to evaluate the performance of the proposed controller.

A comparison was then made between three different FES cycling controllers using experimental results in the same populations. While the controllers varied in their control authority and their method of tracking torque, all controllers demonstrated the ability to accomplish the dual-objective of cadence and power tracking; however, the developed controller exhibited favorable performance and characteristics. These results indicate that cadence should be controlled by the electric motor for all time (i.e., within the FES and KDZ regions) and power should be tracked instantaneously using the large muscle groups of the legs in the FES regions.

Although this article provides a potential rehabilitation strategy for populations with neurological impairments to reduce negative secondary health effects, FES cycling can be further improved. Future work includes investigating an adaptive control scheme for torque control, investigating the effects of modifying cadences and stimulation regions, clinical trials, and accounting for the electromechanical delay observed in neuromuscular electrical stimulation using methods other than empirically based approaches.

ACKNOWLEDGMENT

Any opinions, findings and conclusions, or recommendations expressed in this material are those of the author(s) and do not necessarily reflect the views of the sponsoring agency.

REFERENCES

- C.-W. Peng et al., "Review: Clinical benefits of functional electrical stimulation cycling exercise for subjects with central neurological impairments," J. Med. Biol. Eng., vol. 31, no. 1, pp. 1–11, 2011.
- [2] A. T. Harrington, C. G. A. McRae, and S. C. K. Lee, "Evaluation of functional electrical stimulation to assist cycling in four adolescents with spastic cerebral palsy," *J. Pediatrics*, vol. 2012, pp. 1–11, 2012.
- [3] L. Griffin et al., "Functional electrical stimulation cycling improves body composition, metabolic and neural factors in persons with spinal cord injury," J. Electromyogr. Kinesiol., vol. 19, no. 4, pp. 614–622, 2009. [Online]. Available: http://www.sciencedirect.com/science/article/pii/ S1050641108000436
- [4] V. R. Edgerton et al., "Retraining the injured spinal cord," J. Physiol., vol. 533, no. 1, pp. 15–22, 2001.
- [5] V. R. Edgerton and R. R. Roy, "Paralysis recovery in humans and model systems," *Current Opinion Neurobiol.*, vol. 12, no. 6, pp. 658–667, 2002.
- [6] K. J. Hunt, D. Hosmann, M. Grob, and J. Saengsuwan, "Metabolic efficiency of volitional and electrically stimulated cycling in able-bodied subjects," Med. Eng. Phys., vol. 35, no. 7, pp. 919–925, Jul. 2013.
- [7] K. J. Hunt, J. Fang, J. Saengsuwan, M. Grob, and M. Laubacher, "On the efficiency of FES cycling: A framework and systematic review," *Technol. Health Care*, vol. 20, no. 5, pp. 395–422, 2012.

- [8] M. Grohler, T. Angeli, T. Eberharter, P. Lugner, W. Mayr, and C. Hofer, "Test bed with force-measuring crank for static and dynamic investigations on cycling by means of functional electrical stimulation," *IEEE Trans. Neural Syst. Rehabil. Eng.*, vol. 9, no. 2, pp. 169–180, Jun. 2001.
- [9] H. Kawai, M. J. Bellman, R. J. Downey, and W. E. Dixon, "Closed-loop position and cadence tracking control for FES-cycling exploiting pedal force direction with antagonistic biarticular muscles," *IEEE Trans. Control Syst. Tech.*, vol. 27, no. 2, pp. 730–742, Mar. 2019.
- [10] D. J. Newham and N. de N. Donaldson, "FES cycling," J. Autom. Control, vol. 18, no. 2, pp. 73–76, 2008.
- [11] L. D. Duffell, N. de Neufville Donaldson, and D. J. Newham, "Power output during functional electrically stimulated cycling in trained spinal cord injured people," *Neuromod. Technol. Neural Interface*, vol. 13, no. 1, pp. 50–57, 2010.
- [12] L. D. Duffell et al., "Long-term intensive electrically stimulated cycling by spinal cord-injured people: Effect on muscle properties and their relation to power output," Muscle Nerve, vol. 38, no. 4, pp. 1304–1311, 2008.
- [13] A. J. van Soest, M. Gföhler, and L. J. Casius, "Consequences of ankle joint fixation on FES cycling power output: A simulation study," *Med. Sci. Sports Exerc.*, vol. 37, no. 5, pp. 797–806, 2005.
- [14] C. Fornusek and G. M. Davis, "Maximizing muscle force via low-cadence functional electrical stimulation cycling," J. Rehabil. Med., vol. 36, no. 5, pp. 232–237, 2004.
- [15] J. Szecsi, A. Straube, and C. Fornusek, "Comparison of the pedalling performance induced by magnetic and electrical stimulation cycle ergometry in able-bodied subjects," *Med. Eng. Phys.*, vol. 36, no. 4, pp. 484–489, 2014.
- [16] D. Newham and N. D. N. Donaldson, "FES cycling," in Operative Neuromodulation. Vienna, Austria: Springer, 2007, pp. 395–402.
- [17] J. Szecsi, P. Krause, S. Krafczyk, T. Brandt, and A. Straube, "Functional output improvement in FES cycling by means of forced smooth pedaling," Med. Sci. Sports Exerc., vol. 39, no. 5, pp. 764–780, May 2007.
- [18] C. A. Coste and P. Wolf, "FES-cycling at cybathlon 2016: Overview on teams and results," Artif. Organs, vol. 42, no. 3, pp. 336–341, 2018.
- [19] E. Ambrosini, S. Ferrante, G. Ferrigno, F. Molteni, and A. Pedrocchi, "Cycling induced by electrical stimulation improves muscle activation and symmetry during pedaling in hemiparetic patients," *IEEE Trans. Neural Syst. Rehabil. Eng.*, vol. 20, no. 3, pp. 320–330, May 2012.
- [20] K. J. Hunt et al., "Control strategies for integration of electric motor assist and functional electrical stimulation in paraplegic cycling: Utility for exercise testing and mobile cycling," *IEEE Trans. Neural Syst.* Rehabil. Eng., vol. 12, no. 1, pp. 89–101, Mar. 2004.
- [21] A. Farhoud and A. Erfanian, "Fully automatic control of paraplegic FES pedaling using higher-order sliding mode and fuzzy logic control," *IEEE Trans. Neural Syst. Rehabil. Eng.*, vol. 22, no. 3, pp. 533–542, May 2014.
- [22] K. J. Hunt et al., "Comparison of stimulation patterns for FES-cycling using measures of oxygen cost and stimulation cost," Med. Eng. Phys., vol. 28, no. 7, pp. 710–718, 2006.
- [23] P. F. Li et al., "Adaptive neural network control of fes cycling," in Proc. 4th Int. Conf. Bioinf. Biomed. Eng., Jun. 2010, pp. 1–4.
- [24] J. Szecsi, A. Straube, and C. Fornusek, "A biomechanical cause of low power production during FES cycling of subjects with SCI," J. NeuroEng. Rehabil., vol. 11, no. 1, p. 123, 2014.
- [25] M. J. Bellman, T.-H. Cheng, R. J. Downey, C. J. Hass, and W. E. Dixon, "Switched control of cadence during stationary cycling induced by functional electrical stimulation," *IEEE Trans. Neural Syst. Rehabil.* Eng., vol. 24, no. 12, pp. 1373–1383, Dec. 2016.
- [26] M. J. Bellman, R. J. Downey, A. Parikh, and W. E. Dixon, "Automatic control of cycling induced by functional electrical stimulation with electric motor assistance," *IEEE Trans. Autom. Sci. Eng.*, vol. 14, no. 2, pp. 1225–1234, Apr. 2017.
- [27] V. H. Duenas, C. A. Cousin, V. Ghanbari, and W. E. Dixon, "Passivity-based learning control for torque and cadence tracking in functional electrical stimulation (FES) induced cycling," in *Proc. Annu. Amer. Control Conf.*, Jun. 2018, pp. 3726–3731.
- [28] V. H. Duenas, C. A. Cousin, A. Parikh, P. Freeborn, E. J. Fox, and W. E. Dixon, "Motorized and functional electrical stimulation induced cycling via switched repetitive learning control," *IEEE Trans. Control* Syst. Technol., vol. 27, no. 4, pp. 1468–1479, Jul. 2019.
- [29] C. Cousin, V. H. Duenas, C. Rouse, and W. E. Dixon, "Motorized functional electrical stimulation for torque and cadence tracking: A switched Lyapunov approach," in *Proc. IEEE 56th Annu. Conf. Decis.* Control, Dec. 2017, pp. 5900–5905.

- [30] M. Bellman, "Control of cycling induced by functional electrical stimulation: A switched systems theory approach," Ph.D. dissertation, Univ. Florida, Gainesville, FL, USA, 2015.
- [31] E. Ambrosini, S. Ferrante, T. Schauer, G. Ferrigno, F. Molteni, and A. Pedrocchi, "Design of a symmetry controller for cycling induced by electrical stimulation: Preliminary results on post-acute stroke patients," *Artif. Organs*, vol. 34, no. 8, pp. 663–667, 2010.
- Artif. Organs, vol. 34, no. 8, pp. 663–667, 2010.
 [32] C. Fornusek, G. M. Davis, P. J. Sinclair, and B. Milthorpe, "Development of an isokinetic functional electrical stimulation cycle ergometer," Nueromodulation, vol. 7, no. 1, pp. 56–64, 2004.
- [33] D. B. Popović, "Advances in functional electrical stimulation (FES)," J. Electromyogr. Kinesiol., vol. 24, no. 6, pp. 795–802, Dec. 2014.
- [34] M. Ferrarin, F. Palazzo, R. Riener, and J. Quintern, "Model-based control of FES-induced single joint movements," *IEEE Trans. Neural Syst. Rehabil. Eng.*, vol. 9, no. 3, pp. 245–257, Sep. 2001.
- [35] N. Sharma, K. Stegath, C. M. Gregory, and W. E. Dixon, "Nonlinear neuromuscular electrical stimulation tracking control of a human limb," *IEEE Trans. Neural Syst. Rehabil. Eng.*, vol. 17, no. 6, pp. 576–584, Dec. 2009.
- [36] W. E. Dixon, A. Behal, D. M. Dawson, and S. Nagarkatti, Nonlinear Control of Engineering Systems: A Lyapunov-Based Approach. Boston, MA, USA: Birkhauser, 2003.
- [37] A. F. Filippov, "Differential equations with discontinuous right-hand side," Amer. Math. Soc. Transl., vol. 42, no. 2, pp. 199–231, 1964.
- [38] B. Paden and S. Sastry, "A calculus for computing Filippov's differential inclusion with application to the variable structure control of robot manipulators," *IEEE Trans. Circuits Syst.*, vol. CAS-34, no. 1, pp. 73– 82, Jan. 1987.
- [39] H. K. Khalil, Nonlinear Systems, 3rd ed. Upper Saddle River, NJ, USA: Prentice-Hall, 2002.
- [40] M. O. Ibitoye, N. A. Hamzaid, N. Hasnan, A. K. A. Wahab, and G. M. Davis, "Strategies for rapid muscle fatigue reduction during fes exercise in individuals with spinal cord injury: A systematic review," *PLoS ONE*, vol. 11, no. 2, 2016, Art. no. e0149024.
- [41] N. Stefanovic, M. Ding, and L. Pavel, "An application of L₂ nonlinear control and gain scheduling to erbium doped fiber amplifiers," *Control Eng. Pract.*, vol. 15, pp. 1107–1117, Sep. 2007.
- [42] T. Fujinaka, Y. Kishida, M. Yoshioka, and S. Omatu, "Stabilization of double inverted pendulum with self-tuning neuro-PID," in *Proc. IEEE-INNS-ENNS Int. Joint Conf. Neural Netw.*, vol. 4, Jul. 2000, pp. 345–348.
- [43] F. Nagata, K. Kuribayashi, K. Kiguchi, and K. Watanabe, "Simulation of fine gain tuning using genetic algorithms for model-based robotic servo controllers," in *Proc. Int. Symp. Comput. Intell. Robot. Automat.*, Jun. 2007, pp. 196–201.
- [44] N. J. Killingsworth and M. Krstić, "PID tuning using extremum seeking: Online, model-free performance optimization," *IEEE Control Syst. Mag.*, vol. 26, no. 1, pp. 70–79, Feb. 2006.
- [45] R. Kelly, V. Santibanez, and A. Loria, Control of Robot Manipulators in Joint Space. London, U.K.: Springer, 2005.
- [46] R. J. Downey, E. Ambrosini, S. Ferrante, A. Pedrocchi, W. E. Dixon, and G. Ferrigno, "Asynchronous stimulation with an electrode array reduces muscle fatigue during FES cycling," in *Proc. Int. Func. Elect. Stimul.* Soc., Banff, AB, Canada, Sep. 2012, pp. 154–157.
- [47] R. Kamalapurkar, N. Fischer, S. Obuz, and W. E. Dixon, "Time-varying input and state delay compensation for uncertain nonlinear systems," *IEEE Trans. Autom. Control*, vol. 61, no. 3, pp. 834–839. Mar. 2016.
- IEEE Trans. Autom. Control, vol. 61, no. 3, pp. 834–839, Mar. 2016.
 [48] S. Obuz, R. J. Downey, J. R. Klotz, and W. E. Dixon, "Unknown time-varying input delay compensation for neuromuscular electrical stimulation," in Proc. IEEE Multi-Conf. Syst. Control, Sydney, NSW, Australia, Sep. 2015, pp. 365–370.
- [49] S. Obuz, J. R. Klotz, R. Kamalapurkar, and W. Dixon, "Unknown time-varying input delay compensation for uncertain nonlinear systems," *Automatica*, vol. 76, pp. 222–229, Feb. 2017.



Christian A. Cousin received the Ph.D. degree from the University of Florida, Gainesville, FL, USA, in May 2019.

He was with the Department of Mechanical Engineering, The University of Alabama, Tuscaloosa, AL, USA, as a Faculty Member in July 2019. His current research interests include nonlinear and adaptive control, switched and hybrid systems, cyber-physical systems, hybrid exoskeletons, functional electrical stimulation, human-robot interaction, rehabilitation, and machine learning.

Dr. Cousin was awarded a National Science Foundation Graduate Research Fellowship in 2016.



Victor H. Duenas received the Ph.D. degree from the Department of Mechanical and Aerospace Engineering, University of Florida, Gainesville, FL, USA, in 2018.

In 2018, he joined the Department of Mechanical and Aerospace Engineering, Syracuse University, Syracuse, NY, USA, as an Assistant Professor. His current research interests include nonlinear and adaptive control for rehabilitation robotics, neuromuscular control, and human-robot interaction.



Courtney A. Rouse received the Ph.D. degree in mechanical engineering from the University of Florida, Gainesville, FL, USA, in 2019. Her Ph.D. dissertation focused on control of motorized functional electrical stimulation exercises for neuromuscular therapy.

She is currently a Research Engineer with the Intelligent Systems Division, Southwest Research Institute, San Antonio, TX, USA.



Matthew J. Bellman received the bachelor's, master's, and Ph.D. degrees in mechanical engineering from the University of Florida, Gainesville, FL, USA

He joined the Nonlinear Controls and Robotics Group as an undergraduate and continued research with the group throughout his graduate career. His current research interests include human movement and include robotic exoskeletons, high-performance prosthetics, and functional electrical stimulation (FES). His doctoral dissertation was focused on the

control of human muscle via FES for the purpose of rehabilitating people with paralysis. Now, Dr. Bellman is the co-founder and Chief Technology Officer of MYOLYN, a medical technology company that combines robotics and electrical stimulation to improve health and human performance, where he is responsible for product development, quality management, and regulatory affairs.



Paul Freeborn received the B.S. degree in exercise science from Jacksonville University, Jacksonville, FL, USA, in 2014.

He is currently an Exercise Physiologist and the Center Coordinator for the Brooks Rehabilitation Motion Analysis Center, Jacksonville, FL, USA. His current research interest includes restoration of function after neurological injury or disease by use of innovative technologies that promote functional neurorecovery, such as electrical stimulation and robotics devices.



Emily J. Fox is currently a Research Assistant Professor with the Department of Physical Therapy, University of Florida, Gainesville, FL, USA, and the Director of Neuromuscular Research and the Brooks Rehabilitation Motion Analysis Center, Jacksonville, FL, USA. The objective of her research program is to advance rehabilitation strategies for individuals with neurologic conditions. She focuses on strategies to advance locomotion and respiration after human spinal cord injury and stroke. Her current research interests include the development

of innovative strategies, such as functional electrical stimulation, that are cost-effective and have real-world potential to promote functional recovery.



Warren E. Dixon received the Ph.D. degree from the Department of Electrical and Computer Engineering, Clemson University, Clemson, SC, USA, in 2000.

He was a Research Staff Member and Eugene P. Wigner Fellow with the Oak Ridge National Laboratory (ORNL) until 2004, when he joined the University of Florida, Gainesville, FL, USA, where he is currently a Newton C. Ebaugh Professor with the Mechanical and Aerospace Engineering Department. His current research

interest includes the development and application of Lyapunov-based control methods for uncertain nonlinear systems.

Dr. Dixon is an ASME Fellow. From 2017 to 2018 and 2012 to 2013, his work has been recognized by the University of Florida College of Engineering Doctoral Dissertation Mentoring Award, 2015 and 2009 American Automatic Control Council (AACC) O. Hugo Schuck (Best Paper) Award, the 2013 Fred Ellersick Award for Best Overall MILCOM Paper, the 2011 American Society of Mechanical Engineers (ASME) Dynamics Systems and Control Division Outstanding Young Investigator Award, the 2006 IEEE Robotics and Automation Society (RAS) Early Academic Career Award, an NSF CAREER Award from 2006 to 2011, the 2004 Department of Energy Outstanding Mentor Award, and the 2001 ORNL Early Career Award for Engineering Achievement.